Journal of Water Resource and Protection, 2024, 16, 328-360
https://www.scirp.org/journal/jwarp
ISSN Online: 1945-3108
ISSN Print: 1945-3094

Debris Fan Produced by Failure of Canyon-Blocking Pyroclastic Flows

Michael L. Cummings

Department of Geology, Portland State University, Portland, Oregon, USA
Email: Cummingsm@pdx.edu

How to cite this paper: Cummings, M.L. (2024) Debris Fan Produced by Failure of Canyon-Blocking Pyroclastic Flows. *Journal of Water Resource and Protection*, **16**, 328-360.
https://doi.org/10.4236/jwarp.2024.165019

Received: March 29, 2024
Accepted: May 10, 2024
Published: May 13, 2024

Abstract

Ash-rich pyroclastic flows from the cataclysmic eruption of Mount Mazama (~7700 yr. B. P.), Cascade volcanic arc, Oregon, entered and blocked the narrow, bedrock-lined canyon of the Williamson River approximately 35 to 44 km from the source volcano. The blockage impounded a body of water which then released producing four stratigraphic units in the downstream debris fan. The four stratigraphic units are a boulder core comprised of locally sourced bedrock boulders and three sand-rich units including a fine-grained sand unit, a sandy pumice gravel (±basalt/hydrovolcanic tuff) unit, and a pumice pebble-bearing, crystal-rich sand unit. Hand-drilled auger holes up to ~1.6 m deep were used to obtain samples of the sand-rich units. Units were delimited using surface and down-hole observations, composition and texture, estimated density, statistical parameters of grain size, and vertical and lateral distribution of properties. Overtopping followed by rapid incision into the ash-rich pyroclastic flows progressively cleared the canyon, but a bedrock knickpoint near the head of the canyon limited the volume of debris available for transport to about 0.04 km^3 to 0.08 km^3. Co-deposition of bedrock boulders and lithic-rich sand was followed by rapid deposition with minimal reworking of remobilized pyroclastics. Continued draining of the impounded lake sent hyperconcentrated flows onto the debris fan depositing pumice-rich gravels that graded upward to crystal-rich sands.

Keywords

Outburst Flood, Mount Mazama, Debris Fan, Canyon Blockage, Pyroclastic Flows

1. Introduction

Landscapes east of the Cascades volcanic arc in south central Oregon (**Figure 1**) were blanketed by Plinian pumice fall and locally inundated by unwelded

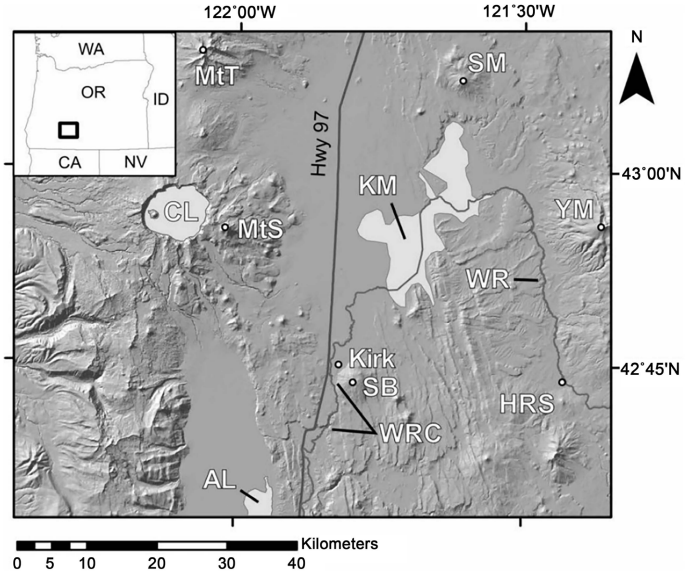

Figure 1. The Williamson River (WR) flows south from Klamath Marsh (KM) through the bedrock-lined Williamson River canyon (WRC). Pyroclastic flows from the eruption of Mount Mazama (a.k.a. Crater Lake (CL)) inundated valleys surrounding the volcano. The flows entered and blocked the Williamson River canyon approximately 35 km to 44 km from its source. MtS = Mount Scott, MtT = Mount Thielsen, SB = Soloman Butte, SM = Sugarpine Mountain, YM = Yamsay Mountain, AL = Agency Lake, HRS = Head of the River Springs.

pyroclastic flows during the ~7700 yr. B.P. cataclysmic eruption of Mount Mazama [1] [2] [3] [4] [5]. These landscapes are comprised of volcanic centers of variable volume and composition, volcaniclastic sedimentary rocks [6], fault scarps of the Central Oregon fault zone [7] [8] [9], and a few narrow bedrock-lined canyons between tectonic, sediment-filled basins. Outlets for Sycan and Klamath marshes pass through such canyons. Both canyons were blocked by pyroclasts from the eruption of Mount Mazama and experienced outburst floods that cleared these obstructions. Wind-remobilized Plinian pumice fall was speculated to have blocked the outlet canyon from Sycan Marsh approximately 80 km east southeast of the source volcano [10] [11]. Unwelded pyroclastic flows from collapse of the Plinian eruption column and the ring-vent phase of the eruption [4] blocked the Williamson River canyon, outlet from Klamath Marsh, approximately 35 km to 44 km from the source volcano (**Figure 1**) [12] [13]. Upstream from the blockage a shallow lake with maximum aerial extent estimated at 590 km^2 [12] developed over the pyroclastic flows and Plinian pumice fall. Failure of this blockage produced a debris fan at the exit of the Williamson River canyon.

The goals of this study were to 1) characterize and determine relations among components of the debris fan; 2) infer depositional processes that produced these components; and 3) from this information refine a conceptual model for removal of the blockage within the canyon.

2. Background

U.S. Geological Survey Ed-Map-supported geologic mapping south of Klamath Marsh by [12] (Wocus Bay quadrangle) and the Williamson River canyon by [14] (Soloman Butte quadrangle) indicated that the bedrock-lined canyon of the Williamson River had been blocked by unwelded pyroclastic flows during the ring-vent phase of the eruption of Mount Mazama. This dam was removed when the impounded lake drained through the canyon [12] [13] [15]. A post-eruption lake and quick draining of that lake were first hypothesized from anomalously thin Plinian pumice fall below about 1395 m, exposed bedrock in narrow valleys where meters of pumice were missing, and a Pleistocene strath terrace stripped of pumice in the southern Klamath Marsh (**Figure 1**). Conaway [12] recognized the link between these features and bedrock boulders at the exit of the Williamson River canyon.

Conaway [12] assumed an outburst flood was initiated when the impounded lake overtopped the pyroclastic dam. Based on this assumption, Conaway [12] estimated peak discharge based on flow competence [16] [17] [18] [19], an empirically based dam-break analogy [20], and a physically based dam-break model [21]. Conaway [12] measured the intermediate axis diameter of boulders in a small quarry at the exit of the Williamson River canyon to estimate peak discharge based on flow competence [16] [17] [18] [19]. The regression analysis with potential energy as the independent variable for a landslide dam-break presented by [20] and later updated by [21] and [22] was used to estimate peak discharge for the empirically based dam-break model. The erosion rate of the pyroclastic dam [22] [23] [24], height of the dam crest relative to dam base, and volume drained at the dam breach were used to estimate peak discharge based on the physically based dam-break model [21].

In 2016, the study reported herein was initiated and focused on the low relief debris fan located between the canyon exit and U.S. Highway 97 (**Figure 2**), a distance of about 4.4 km. Preservation in map view of significant portions of the debris fan provided opportunity to reconstruct the relations among the geology of the canyon, pyroclastic deposits that blocked the canyon, and potential mechanisms for clearing of the canyon. In the discussion, the outburst flood hypothesized by [12] [13] is modified based on data presented herein.

3. Methods

The lack of natural exposures of the debris fan influenced the methods applied to the study of this deposit. A small quarry, slash-burn piles constructed during logging operations, and the modern channel of the Williamson River where it crosses the debris fan provided information within about 2.0 km of the canyon exit. However, in most areas, hand-drilled auger holes were used to determine stratigraphy and collect samples. Unfortunately, this method did not preserve sedimentary structures that are commonly used in similar deposits to infer transport and depositional processes (e.g., [25]-[31]).

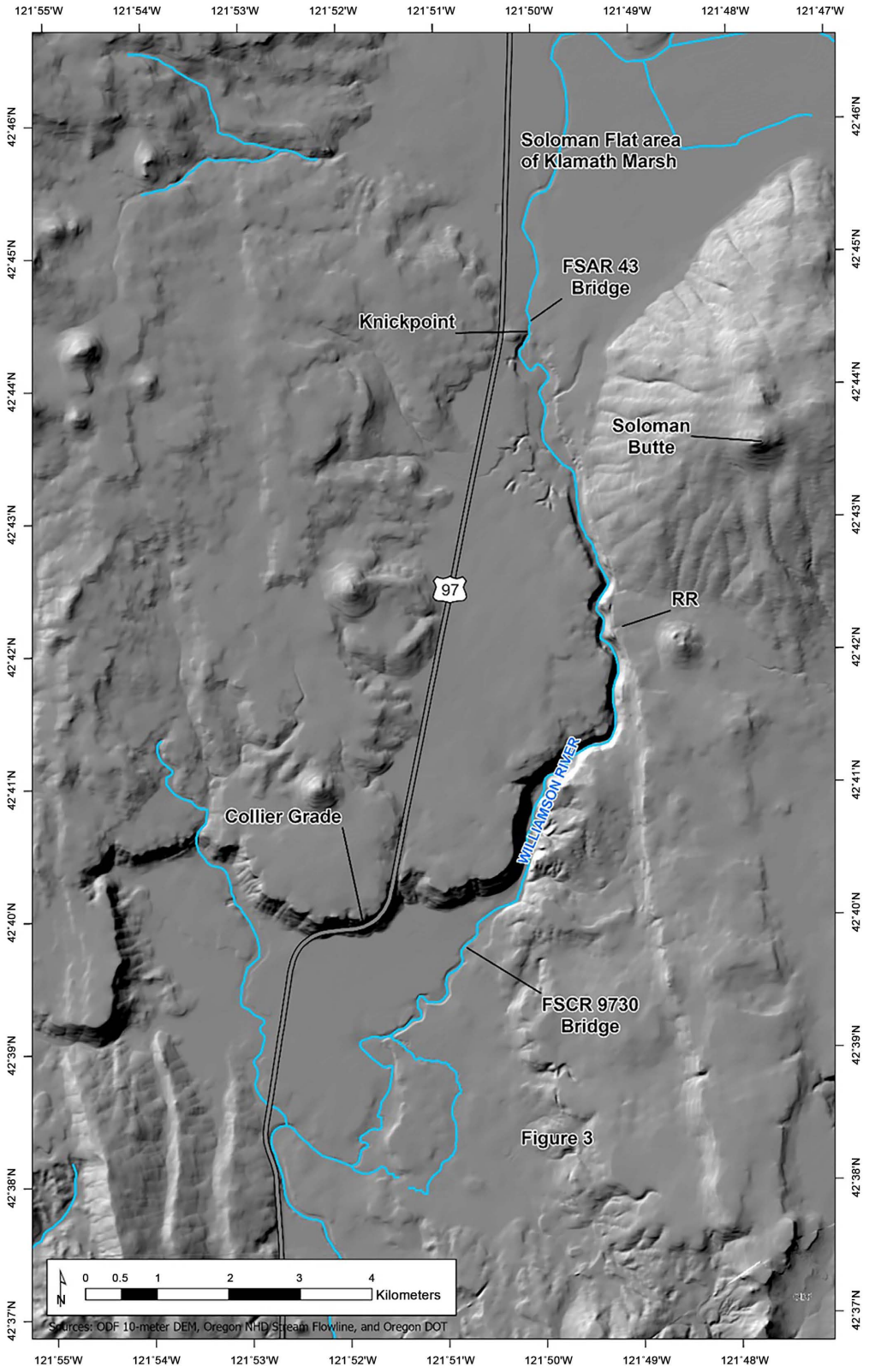

Figure 2. Digital elevation model of the Williamson River canyon. FSAR 43 Bridge = bridge over the Williamson River on Forest Service Arterial Road 43. FSCR 9730 Bridge = bridge over the Williamson River on Forest Service Collector Road 9730. RR = railroad cut where pyroclastic flows overlie Plinian pumice fall which overlies paleosol developed on olivine basalt flows.

One to four samples were collected from each auger hole. The first sample was usually collected from 25 to 40 cm below the ground surface. This depth was greater than near-surface disturbance due to human activity and where moisture content provided enough cohesion to recover a sample in the auger. The depth of auger holes was controlled by obstructions, such as boulders (refusal), or loss of sample during retrieval of the auger due to low cohesion (usually pumice pebble-rich sand). Each sample captured a 4 cm to 6 cm depth span. Sample numbers are based on the last four digits of the Easting and Northing UTM coordinates (e.g., 0593341 E., 4723898 N., Zone 10 = auger hole 3341/3898). Distances within the debris fan were calculated relative to an arbitrary point at the approximate upstream limit of the bedrock boulder deposit within the canyon exit (0595222 E., 4724936 N., Zone 10).

Samples were dried (70˚C) for two to five days before sieving. Sieve sizes were pan, 0.07 mm, 0.25 mm, 0.42 mm, 0.84 mm, 2.00 mm, 4.75 mm, 12.47 mm, 19.03 mm, and 50.8 mm. Modified Wentworth size classes are used in this paper. The mass of each sub-sample was determined, and statistical parameters of grain size were calculated after [32]. Estimated density of each sub-sample was calculated from the mass and volume estimated after tapping on the wall of a 100 ml graduated cylinder to induce compaction. The volume estimates for sub-samples in the pebble size ranges are poorly constrained. Each sample (n = 679) from each auger hole (n = 93) was examined under a binocular microscope to determine composition and visually estimate the percentage of each compositional component.

4. Canyon Setting and Morphology

The Williamson River flows southward from Klamath Marsh through a narrow, 9.2 km long, bedrock-lined canyon (**Figure 1** and **Figure 2**). At 3.7 km downstream from a bedrock knickpoint near Kirk (**Figure 1**) starts the narrow reach of the canyon. Here, the canyon is 210 m to 225 m wide at the rim and 35 m to 40 m deep and incised into basaltic andesite lava flows overlain by olivine basalt flows [14]. After another 1.5 km is a sharp bend where the canyon swings to the west and crosses from lava flows to palagonitized hydrovolcanic tuff. The slope of the bed increases from approximately 0.004 to 0.026 across the contact. Slope decreases again near the canyon exit where the modern river crosses bedrock boulders in the debris fan. The last 4 km of the canyon is incised (60 m to 95 m deep; 270 m to 400 m wide) into eroded hydrovolcanic tuff which is overlain on the west side by a basaltic andesite intracanyon lava flow. The river drops from 1372 m near the knickpoint to approximately 1280 m at the canyon exit.

The pumice fall during the Plinian phase of the Mount Mazama eruption [1] [2] [4] [5] was deposited in an eastern and a north-northeastern lobe [1] [2]. The Williamson River canyon lies south of and peripheral to the thickest accumulation of pumice in the eastern lobe. Contours of constant thickness for the pumice deposit presented by [2] cross the canyon at high angles. The combined

thickness of the lower and upper pumice units [2] thinned from approximately 140 cm near the knickpoint to 40 cm near the canyon exit.

The Plinian pumice fall is overlain by pyroclastic flows that were deposited during collapse of the Plinian eruption column and the multiple-vent phase of the eruption [1] [2] [4] [5]. Along the southern margin of the area inundated by pyroclastic flows, volcanic cones (e.g., Soloman Butte, **Figure 2**) funneled these flows into valleys including the Williamson River canyon and neighboring plateau. Ash-rich pyroclastic flows traveled approximately 35 km before entering the upstream end of the Williamson River canyon (**Figure 1**).

The canyon was filled by pyroclastic flows between the knickpoint and somewhat beyond the distinct bend and partially filled to the canyon exit (**Figure 2**). The volume of the blockage is estimated at 0.04 km^3 to 0.08 km^3 based on the depth and width (rim to rim) of the canyon and inferred thickness of the pyroclastic fill. Some pyroclastic flows may have passed through the canyon and came to rest beyond. Pyroclastic flows also crossed the plateau west of the canyon and overshot the south rim of the plateau (**Figure 2**).

The pyroclastic flows were ash-rich; seventy-three to 92 weight percent of samples (n = 5) passed through the 2.00 mm sieve (= volcanic ash) (**Table 1**). The graphic mean grain size (M_z) was +1.40Φ to +2.11Φ, but the greatest mass was retained on the 0.07 mm sieve (30.5 to 53.6 wt. %). Mass distribution was bimodal for four out of five samples. The relatively minor coarser grained mode (0.42 mm) was pumices, and the distinct finer grained mode (0.07 mm) was compact glass and crystals (visually estimated < 5 percent). Samples were coarse (n = 2/5) to strongly coarse (n = 3/5) skewed (−0.19 to −0.34) due to pumice lapilli (>2.00 mm). The estimated density for all grain sizes ranged from 0.4 g/cm^3 to 0.9 g/cm^3. Sorting ranged from poor to very poor (1.72Φ to 2.49Φ).

5. Debris Fan

Remnants of the debris fan lie at elevations near 1285 m and were examined between the canyon exit and U.S. Highway 97, approximately 4.4 km. The debris fan includes a core of bedrock boulders that extends at least 1.9 km from the canyon exit and pumice pebble-bearing sand which overlies, flanks, and extends beyond the bedrock boulder core (**Figure 3**). Remnants of the palaeosurface are identified in the field by isolated boulders of pumice resting upon the modern surface. The diameter of these pumice boulders is far greater than pumices encountered in auger holes. The greatest area of paleosurface is preserved north of the Williamson River as a subtle ridge from approximately 2 km to at least U.S. Highway 97 (**Figure 3**). The ridge is dissected by ephemeral streams that locally are incised to bedrock. Extending from the canyon exit is a network of abandoned channels left by the Williamson River as it migrated to its current location. Channel migration eroded part of the debris fan, exposed part of the boulder core, and locally produced a lag deposit of stream rounded basalt pebbles and cobbles in crystal-rich, medium- to coarse-grained sand. Eventually, the

Table 1. Summary of grain size characteristics and grain size distributions in pyroclastic and sand-rich stratigraphic units.

Pyroclastic flows (n = 5)				
Physical parameter	**Range of values**	**Average; Standard deviation**	**Statistical parameters (Folk, 1980)**	**Range of values**
Bimodal	4 of 5		M_z	1.43 - 2.11Φ
Greatest wt. %	0.07 mm, 5 of 5		Sorting ($б_I$)	1.72 to 2.49Φ
wt. % gravel	8.3 to 18.3 wt. %	12.2; 3.8	Skewness: Coarse	2 of 5
wt. % sand	64.8 to 84.9 wt. %	75.6; 9.5	(Sk_I) St. Coarse	3 of 5
Est. density (bulk)	0.6 to 0.8 g/cm^3	0.7; 0.1	Kurtosis (K_G):	
Est. density (fine sand)	0.8 to 0.9 g/cm^3	0.8; 0.1	Mesokurtic	4 of 5
Est. density (coarse sand)	0.5 to 0.8 g/cm^3	0.7; 0.1	Leptokurtic	1 of 5
Fine-grained sand unit (n = 14)				
Bimodal	7 of 14		M_z	0.84 to 2.10Φ
	0.07 mm, 12 of 14		Sorting ($б_I$)	1.57 to 2.41Φ
Greatest wt. %	0.25 mm, 1 of 14		Skewness: N. sym.	4 of 14
	0.42 mm, 1 of 14		(Sk_I) Coarse	9 of 14
wt. % gravel	5.4 to 20.9 wt. %	12.1; 5.0	St. coarse	1 of 14
wt. % sand	65.8 to 89.6 wt. %	81.6; 7.1	Kurtosis (K_G):	
Est. density (bulk)	0.6 to 0.7 g/cm^3	0.6; 0.04	Platykurtic	5 of 14
Est. density (fine sand)	0.9 to 1.2 g/cm^3	1.0; 0.1	Mesokurtic	5 of 14
Est. density (coarse sand)	0.4 to 0.7 g/cm^3	0.5; 0.1	Leptokurtic	4 of 14
Sandy pumice gravel (±basalt/hydrovolcanic tuff) unit < 2.0 km (n = 10)				
Bimodal	4 of 10		M_z	−0.31 to 1.55Φ
	0.25 mm, 1 of 10		Sorting ($б_I$)	1.24 to 2.35Φ
Greatest wt. %	0.42 mm, 6 of 10		Skewness: St. fine	1 of 10
	0.84 mm, 3 of 10		(Sk_I) Fine	2 of 10
wt. % gravel	3.5 to 35.9 wt. %	18.5; 10.6	N. sym.	3 of 10
wt. % sand*	61.4 to 89.6 wt. %	76.4; 9.0	Coarse	3 of 10
Est. density (bulk)	1.1 to 1.4 g/cm^3	1.2; 0.1	St. Coarse	1 of 10
Est. density (fine sand)	1.1 to 1.4 g/cm^3	1.2; 0.1	Kurtosis (K_G):	
			Platykurtic	1 of 10
Est. density (coarse sand)	1.2 to 1.9 g/cm^3	1.3; 0.2	Leptokurtic	6 of 10
			V. Leptokurtic	2 of 10
2.0 to 3.6 km (n = 21)				
Bimodal	16 of 21		M_z	−1.48 to 0.45Φ
	0.25 mm, 2 of 21		Sorting ($б_I$)	1.52 to 2.64Φ
	0.42 mm, 6 of 21		Skewness: St. fine	2 of 21
Greatest wt. %	0.84 mm, 2 of 21		(Sk_I) Fine	3 of 21
	2.00 mm, 7 of 21		N. sym.	9 of 21
	4.75 mm, 4 of 21		Coarse	7 of 21
wt. % gravel	18.2 to 69.0 wt. %	39.6; 14.0	Kurtosis (K_G):	
wt. % sand	29.6 to 80.3 wt. %	57.7; 14.2	Platykurtic	9 of 21
Est. density (bulk)	0.4 to 1.1 g/cm^3	0.6; 0.2	Mesokurtic	10 of 21
Est. density (fine sand)	0.7 to 1.2 g/cm^3	1.0; 0.2	Leptokurtic	2 of 21
Est. density (coarse sand)	0.4 to 1.2 g/cm^3	0.7; 0.2		

Continued

>3.7 km (n = 5)				
Bimodal	4 of 5		M_z	−0.33 to 0.47Φ
Greatest wt. %	0.84 mm, 4 of 5 4.75 mm, 1 of 5		Sorting ($б_I$) Skewness: St. fine	1.23 to 2.88Φ 1 of 5
wt. % gravel	11.2 to 42.6 wt. %	25.1; 13.2	(Sk_I) Fine	3 of 5
wt. % sand	45.2 to 86.5 wt. %	68.4; 15.7	N. Sym.	1 of 5
Est. density (bulk)	0.4 to 0.7 g/cm^3	0.6; 0.1	Kurtosis (K_G):	
Est. density (fine sand)	0.6 to 1.1 g/cm^3	0.8; 0.2	Platykurtic	1 of 5
Est. density (coarse sand)	0.4 to 0.7 g/cm^3	0.6; 0.1	Mesokurtic	2 of 5
			Leptokurtic	2 of 5
Pumice pebble-bearing, crystal-rich sand unit 0.9 to 1.2 km (n = 4)				
Bimodal	None		M_z	0.90 to 1.21Φ
Greatest wt. %	0.42 mm, 4 of 4		Sorting ($б_I$)	0.68 to 1.02Φ
wt. % gravel	0.3 to 2.9 wt. %	1.2; 1.2	Skewness: Fine	3 of 4
wt. % sand	95.9 to 99.6 wt. %	97.5; 1.6	(Sk_I) N. Sym	1 of 4
Est. density (bulk)	1.3 to 1.4 g/cm^3	1.3; 0.03	Kurtosis (K_G):	
Est. density (fine sand)	1.3 to 1.4 g/cm^3	1.3; 0.05	Mesokurtic	2 of 4
Est. density (coarse sand)	1.3 to 1.4 g/cm^3	1.3; 0.07	Leptokurtic	2 or 4
1.5 to 3.5 km (n = 32)				
Bimodal	7 of 32		M_z	0.12 to 1.45Φ
Greatest wt. %	0.42 mm, 29 of 32 0.84 mm, 4 of 32*		Sorting ($б_I$) Skewness: Fine	1.01 to 2.09Φ 3 of 32
wt. % gravel	1.0 to 26.8 wt. %	13.4; 6.7	(Sk_I) N. Sym.	15 of 32
wt. % sand	69.0 to 96.5 wt. %	83.8; 7.1	Coarse	13 of 32
Est. density (bulk)	0.6 to 1.3 g/cm^3	1.0; 0.2	St. Coarse	1 of 32
Est. density (fine sand)	0.8 to 1.4 g/cm^3	1.2; 0.1	Kurtosis (K_G):	
Est. density (coarse sand)	0.8 to 1.3 g/cm^3	1.1; 0.2	Mesokurtic	3 of 32
			Leptokurtic	25 of 32
			V. Leptokurtic	4 of 32

*Greatest weight percent was equal on the 0.42 mm and 0.84 mm sieves for sample 3561/3655. Fine sand (≥0.07 mm to <0.42 mm), coarse sand (≥0.42 mm to <2.00 mm), gravel (≥2.00 mm). Skewness: N. Sym = near symmetrical, St. Coarse = strongly coarse, St. Fine = strongly fine.

Williamson River established its channel across the boulder core (Figure 4) and eroded into hydrovolcanic tuff and volcaniclastic sedimentary rocks south of the debris fan. The following sections describe the composition, estimated density, grain size, statistical parameters of grain size, and stratigraphic relations of the debris fan.

5.1. Composition

The composition of the three size groupings used to characterize the deposit are described in this section. The size groupings are: 1) pebbles, cobbles, and boulders (≥2.00 mm), 2) sand (≥0.07 mm <2.00 mm) collected on 0.07 mm, 0.25 mm, 0.42 mm, and 0.84 mm sieves, and 3) very fine-grained sand and silt (<0.07 mm ("silt"). The descriptions are based on field examination of boulders to pebbles, and binocular microscope examination of all size divisions less than 50.8 mm.

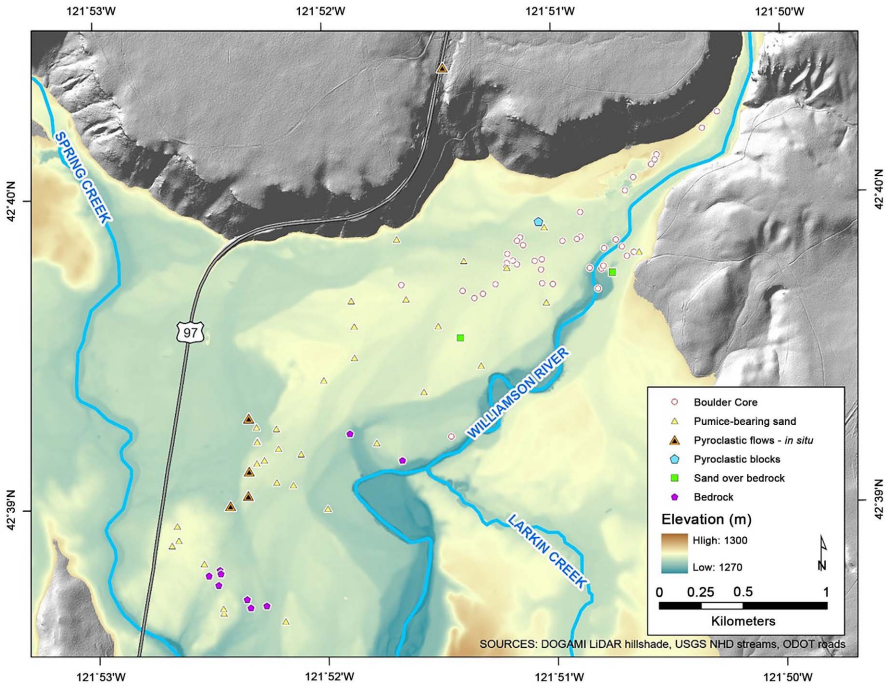

Figure 3. Elevation model for the Williamson River downstream from the canyon exit (upper right). The elevation of the debris fan is approximately 1285 m and partially eroded by the Williamson River, Spring Creek, and ephemeral streams. Open circles indicate locations where bedrock boulders are exposed, are present on slash-burn piles or stopped advancement (refusal) of the hand auger.

Figure 4. Williamson River where it crosses the boulder core upstream from the bridge on FSCR 9730 (**Figure 2**). The cliff (upper left) is a basaltic andesite intracanyon flow that overlies an eroded surface cut into hydrovolcanic tuff (photo by S. Mattenberger).

Binocular microscope observations indicated very fine sand to silt partially infilled vesicles in pumices and partially coated grains. In most cases the fine-grained

coating did not reduce ability to classify grains, however, near the canyon exit and a couple of auger holes along the northern edge of the deposit, coatings made grain identification difficult. All transfers of material from container to container released fines suggesting the masses for <0.07 mm samples are somewhat under reported.

5.1.1. Pebbles, Cobbles, and Boulders (>2.00 mm)

Clasts in the pebbles, cobbles, and boulders size groupings (≥2.00 mm) include 1) porphyritic pumices, 2) olivine basalt, 3) vesicular to massive basaltic andesite (herein referred to as basalt), and 4) hydrovolcanic tuff.

1) Porphyritic pumice occurred in three settings: a) rounded cobbles and boulders (>64 mm) that rest upon the paleosurface of the debris fan, b) rounded cobbles (≥50.8 mm) within the deposit, and c) rounded pebbles (2.00 mm to 19.03 mm) present in all samples collected from auger holes.

a) Where the paleosurface produced by the flood is preserved, isolated, rounded cobbles and boulders of porphyritic pumice are widely dispersed and rest upon the surface between 1.9 km and 4.4 km from the canyon exit. The largest boulders were estimated at 15 to 20 cm in diameter, and all were visibly weathered. These pumice boulders are interpreted as once floating in the impounded lake and were transported to their current location during the waning stages of the flood. Where migration of the Williamson River eroded the debris fan at 1.68 km from the canyon exit, a lens of rounded cobbles and boulders of pumice rests upon the surface. The lens, a bar formed during channel migration, is a single layer approximately 15 m long and 3 m wide. The cobbles and boulders have rough surface textures reflecting the internal stretched glass fabric of pumices.

b) Rounded pumice cobbles (>50.8 mm) are embedded within the deposit. Where present, one or two cobbles were recovered from the auger hole in a single auger run suggesting they occur at discrete horizons. Although vesiculation was prominent, it was not as well developed as in the pumice cobbles and boulders that rested upon the surface of the deposit (a).

c) Rounded pebbles (≥2.00 mm and <19.03 mm) of pumice were present in all samples. Shapes were influenced by the size of vesicles and stretching of the glass fabric. Vesicles and stretched fabric were easily observed with the unaided eye. Density was estimated at 0.3 to 0.5 g/cm^3.

2) Thin (2 to 3 m thick) flows of olivine basalt crop out along the eastern wall of the Williamson River canyon approximately 6 km upstream from the canyon exit [14]. Boulders in the quarry and slash-burn piles were not weathered and, in the quarry, were up to 3.40 m (d_i) [12] (**Figure 5(a)**). Boulders were present at least 1.9 km from the canyon exit. This lithology was distinctly textured with wavy, 2 to 5 cm thick, variably vesiculated bands (**Figure 5(b)**).

3) Dark gray, vesicular to massive basalt lines the narrow reach of the canyon and forms rim rock on the plateau along the west side in the lower reach (**Figure 2**). The size of boulders from these sources is controlled by the spacing of

(a) (b)

Figure 5. a) Boulder of banded olivine basalt in the quarry near the canyon exit (~14 cm × 20 cm field notebook for scale). The nearest outcrops of this lithology relative to the quarry is 6 km. b) Close-up of vesiculation and banding patterns in the olivine basalt (14.5 cm long mechanical pencil in upper left corner for scale).

cooling joints. Rounded pebbles and cobbles of this lithology were collected from auger holes and locally formed a surface lag deposit within about 2.3 km from the canyon exit.

4) Palagonitized basaltic hydrovolcanic tuff boulders (**Figure 6**) were sourced from the lower 4 km of the canyon. Cliff-forming outcrops of proximal and vent facies near the canyon exit were the likely sources of the boulders. The largest tuff boulder in the quarry (**Figure 6**) had d_i = 2.75 m [12]. Boulders were present throughout the bedrock boulder core. These boulders weather to angular rubble. Beyond the bedrock boulder core, this lithology was present as rounded very fine pebbles and in the coarse- and very coarse-sand fractions.

5.1.2. Sand (≥0.07 mm to <2.00 mm)

The sand fraction (≥0.07 mm to <2.00 mm) comprised 30 to 100 weight percent in all samples (n = 90) and, in 63 percent of samples, greater than 75 weight percent. Samples where the weight percent sand fell below about 50 weight percent contained abundant pumice pebbles. In nearly half of the samples the greatest weight percentage was retained on the 0.42 mm sieve (medium- and coarse-grained sand). The composition of sand was simplified to six components: 1) basalt, 2) hydrovolcanic tuff, 3) flow-banded felsics, 4) pumice (variably vesiculated), 5) compact "glass", 6) and crystals (plagioclase, pyroxene, hornblende, apatite, magnetic grains). The composition of sand varied by grain size and distance from the canyon exit. The percentage of each component and subcomponent was visually estimated and compared to density estimates for each size fraction.

5.1.3. Very Fine-Grained Sand and Silt (<0.07 mm) Referred to as "Silt"

Very fine-grained sand and silt (<0.07 mm), "silt", comprised 0.2 to 12.3 weight percent of samples. Approximately 71% of samples contained < 5 weight percent; 25% contained ≥5 <10 weight percent; 4% contained ≥ 10 weight percent. Individual grains were distinct at 60× magnification suggesting very fine-grained sand (0.07 mm to 0.062 mm) and coarse silt (0.062 mm to 0.031 mm) were predominant.

Figure 6. Palagonitized hydrovolcanic tuff boulder. The dimensions of this boulder are d_l = 3.40 m, d_i = 2.75 m [12]. Field notebook for scale (~14 cm × 20 cm). Cliffs formed of this lithology are present within 0.3 km of this boulder exposed in the quarry.

5.2. Composition Versus Density

General relations between composition and estimated density are illustrated by 1) bulk samples and 2) sub-samples according to grain size. Smith and Smith [33] reported 3- to 5-fold range in the specific gravity of grains in recent volcaniclastic sediments (e.g., heavy minerals to strongly vesiculated pumice). They also noted an inverse relation between specific gravity and grain size within clasts of the same composition (e.g., compact glass retained on 0.07 mm sieve to prominently vesiculated pumice pebble and cobbles). Manville *et al.* [34] examined the hydrodynamics of pumice and implications for remobilization of pyroclasts. These properties of the debris fan focused attention on relations among grain size, composition, and estimated density.

Estimated density of bulk samples ranged from 0.4 g/cm^3 to 1.4 g/cm^3 (**Table 1**) and decreased with increasing distance from the canyon exit. These variations reflected changes in the relative proportion of bedrock clasts, crystals/compact glass, pumice vesiculation, and the prominence of pumice pebbles.

5.3. Stratigraphic Divisions

Delimiting stratigraphic units first combined surface and down-hole observations from the field with mass distribution and estimated density with respect to grain size. These provisional units were modified using compositional (visually estimated %) and textural data from observations under a binocular microscope. Synthesis of these data accounted for the range of densities among compositional components (e.g., pyroxene crystals vrs. highly vesiculated pumices) and within components of the same composition (e.g., compact glass vrs. highly vesiculated pumices) [33] [34]. Further refinement of stratigraphic units used statistical parameters of grain size [34] and lateral and vertical distribution of data to define four stratigraphic units. The informal names applied to these units emphasize characteristics that supported field investigations. Generalized units include: 1) boulder core, 2) fine-grained sand, 3) sandy pumice gravel (±basalt/hydrovolcanic

tuff), and 4) pumice pebble-bearing, crystal-rich sand. Contacts among units appear to be gradational over several centimeters (1 to 2 auger returns (4 to 8 cm)) and characteristics vary spatially relative to the canyon exit.

5.3.1. Boulder Core

Bedrock boulders extend from within the canyon (near UTM 0595222 E., 4724936 N., Zone 10) for at least 2.5 km in a west-southwest direction (Figure 3). Bedrock boulders are known from a small quarry near the canyon exit, the channel of the Williamson River where it crosses the boulder core (Figure 4), slash-burn piles constructed during logging operations, and hand-drilled auger holes where bedrock boulders ("refusal") were buried beneath sand-rich sediment (Figure 7). The width at 1.3 km was approximately 420 m. Boulders of basalt, olivine basalt (Figure 5), and hydrovolcanic tuff (Figure 6) were present in slash-burn piles at least to 1.8 km. However, the farthest auger holes where refusal occurred were 2.15 km (3341/3898) and 2.50 km (3639/2994) (Figure 7). At these sites of refusal, the "boulders" were too large to enter the auger and could not be moved by the auger. They may have been isolated boulders in the sandy pumice gravel (±basalt/hydrovolcanic tuff) unit.

Human-caused disturbances and lack of natural exposures impaired an estimate of thickness and identification of materials between boulders. Rough estimates of thickness within the canyon and near the bridge over the Williamson River on FSCR 9730 (Figure 2) were 6 to 7 m and 5 m, respectively. Lithic-rich sand to gravel is inferred to surround the bedrock boulders and to have characteristics similar to the sandy pumice gravel (±basalt/hydrovolcanic tuff) unit. The boulder core is inferred to thin rapidly to the southwest and to overlie hydrovolcanic tuff near the canyon exit and tuffaceous fine-grained sandstone to siltstone at its distal extent. Its distribution is inferred to be influenced by pre-eruption Williamson River channel and floodplain features.

5.3.2. Sand-Rich Units

Three sand-rich stratigraphic units include 1) fine-grained sand, 2) sandy pumice gravel (±basalt/hydrovolcanic tuff), and 3) pumice pebble-bearing, crystal-rich sand. Characteristics of sand-rich units and, for comparison, pyroclastic flows are summarized in Table 1.

1) Fine-grained sand. A poorly sorted unit characterized by abundant fine- to very fine-grained pumice sand, relative size uniformity with low estimated density, few crystals, and few pumice pebbles was first recognized at auger hole 2478/3051 (Figure 7, E.O.H. (end of hole) 160 cm). Sand with similar characteristics was present in 14 samples from 7 auger holes. The fine-grained sand unit was recovered from the deepest levels in three auger holes at 2.46, 2.51, and 2.84 km (Figure 7; 3042/3805, 3060/3652, 2879/3331). It was exposed at 3.33, 3.98, and 4.20 km (Figure 7; 2478/3051, 2653/1891, 2284/1939) and in the sub surface at 4.08 km (Figure 7; 2167/2234). At all sites, the post-flood surface was preserved.

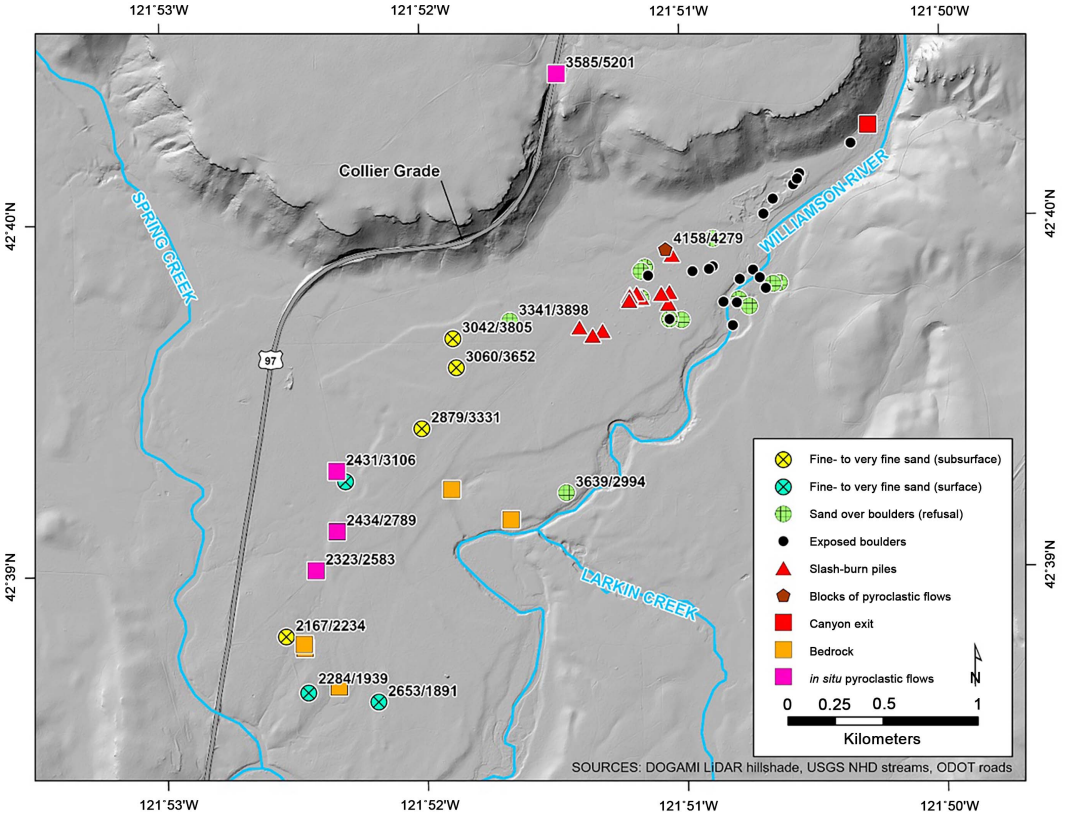

Figure 7. Locations where the boulder core and the fine-grained sand unit were present. The boulder core included exposed bedrock boulders, boulders on slash-burn piles, and sand over boulders (refusal). The fine- to very fine-grained sand unit was present below other units at sites labeled (subsurface) and present at the surface at sites labeled (surface). Sites underlain by *in situ* pyroclastic flows and exposed bedrock are indicated. Sample numbers are those referred to in the text.

The average properties of the fine-grained sand unit (Table 1) suggest it was derived from *in situ* pyroclastic flows and was rapidly deposited with little reworking. Weight percentages and estimated densities of four grain size groups ("silt" (<0.07 mm), fine sand (≥0.07 mm to <0.42 mm), coarse sand (≥0.42 mm to <2.00 mm), gravel (≥2.00 mm)) relative to distance from the canyon exit are presented in Figure 8 and Figure 9, respectively. These four grain-size groups are based on compositional data. Data for pyroclastic flows for the same grain-size groups are included in these figures. The greatest weight percentages and highest estimated densities were recorded for the fine-sand group (≥0.07 mm to <0.42 mm) in both the fine-gained sand unit and the pyroclastic flows. Compact glass was enriched in the fine-sand group at all distances. Downstream from pyroclastic flows exposed at 3.7 km, the weight percentages increased for the fine-sand and "silt" groups suggesting entrainment of finer grained materials from the pyroclastic flows. The greater estimated densities in the fine-sand group in three samples collected up steam of pyroclastic flows exposed at 3.5 and 3.7 km suggest crystals are more abundant in these samples.

2) Sandy Pumice Gravel (± basalt/hydrovolcanic tuff). The sandy pumice gravel (±basalt/hydrovolcanic tuff) unit is distinguished by composition,

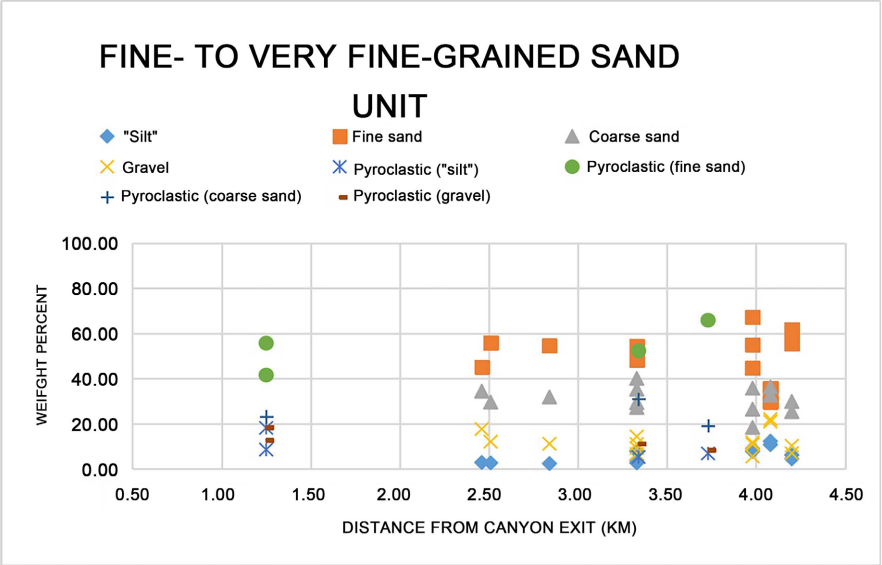

Figure 8. Weight percentages with respect to distance from the canyon exit for the fine-grained sand unit and pyroclastic flows. "Silt" = <0.07 mm; fine sand = ≥0.07 mm <0.42 mm; coarse sand = ≥0.42 mm <2.00 mm); gravel ≥2.00 mm. Average weight percent: "silt" = 6.3%, std. dev. = 3.2; fine sand = 50.7%, std. dev. = 9.7; coarse sand = 30.8%, std. dev. = 5.6; gravel = 12.1%, std. dev. = 5.0.

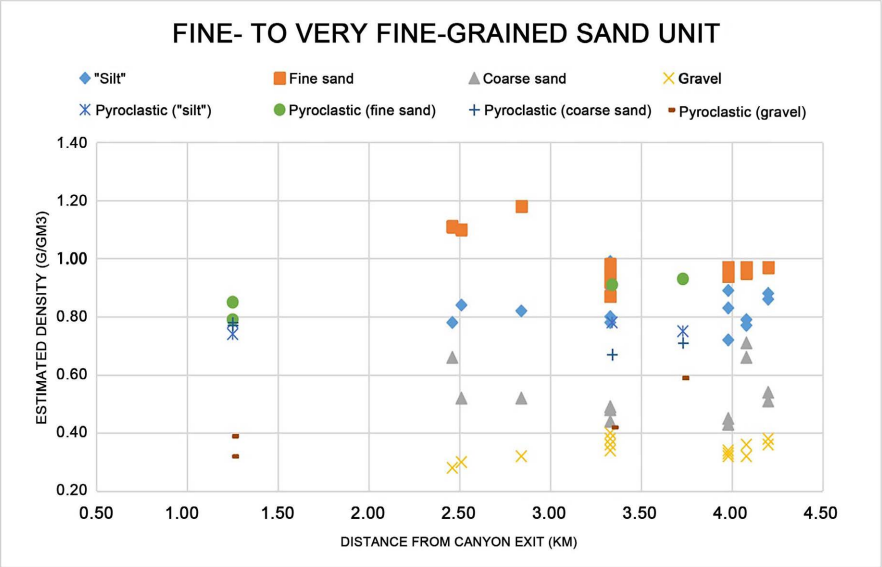

Figure 9. Estimated densities with respect to distance from the canyon exit for the fine-grained sand unit and pyroclastic flows. "Silt" = <0.07 mm; fine sand = ≥0.07 mm <0.42 mm; coarse sand = ≥0.42 mm <2.00 mm; gravel ≥2.00 mm. Average estimated density: "silt" = 0.8 g/cm^3, std. dev. = 0.1; fine sand = 1.0 g/cm^3, std. dev. = 0.1; coarse sand = 0.5 g/cm^3, std. dev. = 0.1; gravel = 0.3 g/cm^3, std. dev. 0.03.

estimated density, statistical parameters of grain size [32], and stratigraphic position. The Williamson River eroded the upper part of this unit within 2.0 km of the canyon exit. The pumice pebble-rich upper part of the unit overlies pyroclastic flows at 3.5 km and 3.7 km. **Figure 10** shows the root ball of a ponderosa pine

Figure 10. Root ball of a ponderosa pine tree (2434/2789) where pumice gravel (left of the yellow notebook) overlies pyroclastic flows (up direction to the left). The site was located upslope from a small ephemeral stream near the crest of the ridge and 3.5 km from the canyon exit.

tree where the contact between pyroclastic flows and the upper pumice pebble-rich part of the unit (3.5 km) is exposed. Pyroclastic flows exposed in a lodgepole pine root ball in an ephemeral stream valley underlies the pumice pebble-rich upper part of the unit at 3.7 km. Unit characteristics are summarized in Table 1 (<2.0 km, 2.0 km to 3.5 km, >3.7 km).

Composition and weight percent gravel (≥2.00 mm) are the most distinctive characteristics (Figure 11). The relative proportions of basalt, hydrovolcanic tuff, and pumice in gravel changes with distance: abundance of basalt and hydrovolcanic tuff clasts decreases while abundance of pumice increases. Basalt and hydrovolcanic tuff clasts in gravel were absent beyond about 2.3 km. The weight percent gravel provided additional definition of the unit. Regardless of composition, greater than 20 weight percent gravel described all but four samples. These four samples were located at less than 1.6 km. At distances greater than 2.0 km, the gravel-rich unit graded upward to the pumice pebble-bearing, crystal-rich sand unit (described below; Figure 11). Bedrock, boulder core, pyroclastic flows, and the fine-grained sand unit are overlain by this unit.

Where migration of the Williamson River eroded the upper portion of the sandy pumice gravel (±basalt/hydrovolcanic tuff) unit (roughly <2.0 km), the unit is overlain by coarse-grained sand, rounded basalt pebbles, and, locally, boulders of pumice. These reworked materials sloughed into auger holes for the first 10 to 20 cm above the depths where samples were collected. In several locations the auger holes were drilled among slash-burn piles where bedrock boulders were exposed. In these areas, depth of refusal was commonly 30 to 50 cm

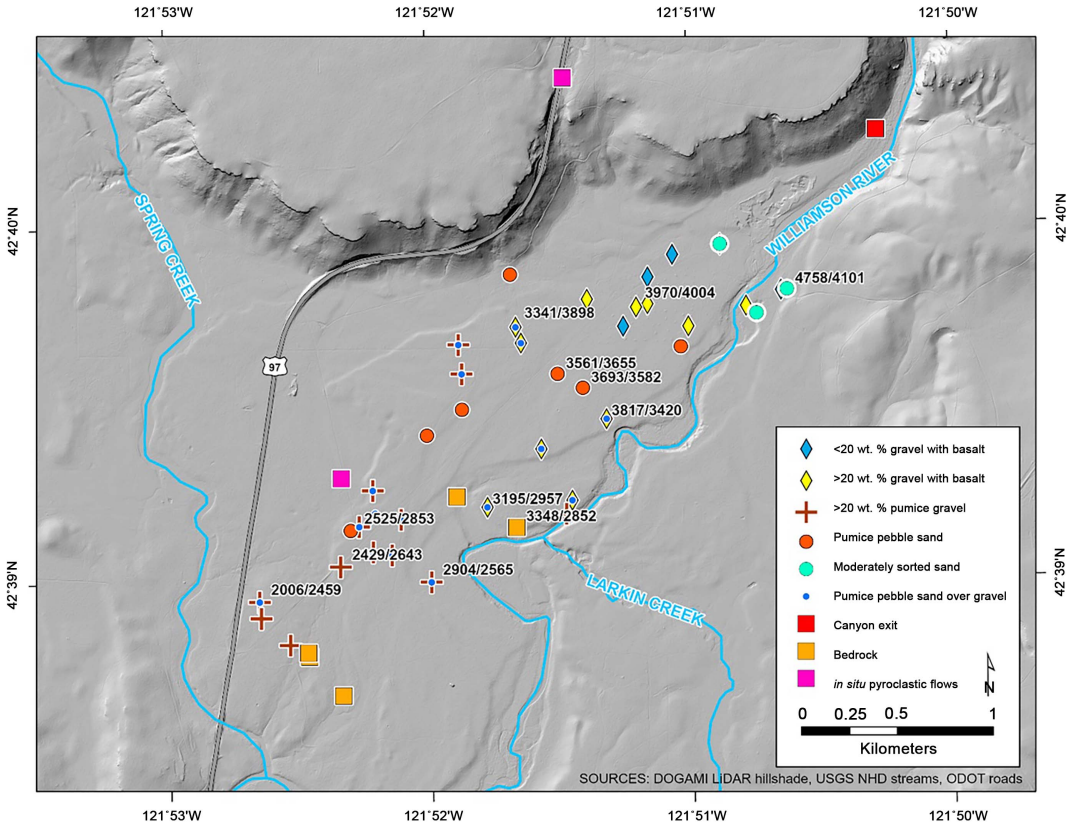

Figure 11. Locations of auger holes that contained the sandy pumice gravel (±basalt/hydrovolcanic tuff) unit and/or the pumice pebble-bearing, crystal-rich sand unit. Auger holes for the sandy pumice gravel (±basalt/hydrovolcanic tuff) are the first three items in the legend (<20 wt. % gravel with basalt, >20 wt. % gravel with basalt, and >20 wt. % pumice gravel). Locations of auger holes that contained the pumice pebble-bearing, crystal-rich sand unit include 1) pumice pebble-bearing, crystal-rich sand (pumice pebble sand), 2) moderately to moderately well-sorted sand between 0.9 and 1.2 km from the canyon exit (moderately sorted sand), 3) pumice pebble-bearing, crystal-rich sand overlying the sandy pumice gravel (±basalt/hydrovolcanic tuff) (pumice pebble sand over gravel).

(sand over boulders (refusal) in Figure 7). Farther from the canyon exit and laterally with respect to the boulder core, auger holes penetrated to greater depth with or without refusal, abundance of pumice pebbles increased, but basalt and hydrovolcanic tuff were present in coarse-grained sand and pebbles.

Between 2.0 and 3.5 km, auger holes sampled the upper part of the sandy pumice gravel (±basalt/hydrovolcanic tuff) unit and were characterized by abundant pumice (Table 1). Stratigraphic relations determined from three auger holes (3341/3898 (2.15 km), 2904/2565 (3.32 km), and 2429/2643 (3.61 km); Figure 11) located where isolated pumice boulders were present at the surface indicate that over 1.38 km and 1.55 km, respectively, gravel changed from pumice with basalt and hydrovolcanic tuff pebbles at 3341/3898 to pumice pebbles at 2904/2565 and 2429/2643.

Weight percentages and estimated densities for the sandy pumice gravel (± basalt/hydrovolcanic tuff) unit with respect to distance from the canyon exit are presented in Figure 12 and Figure 13. Weight percentages reflect the abundance

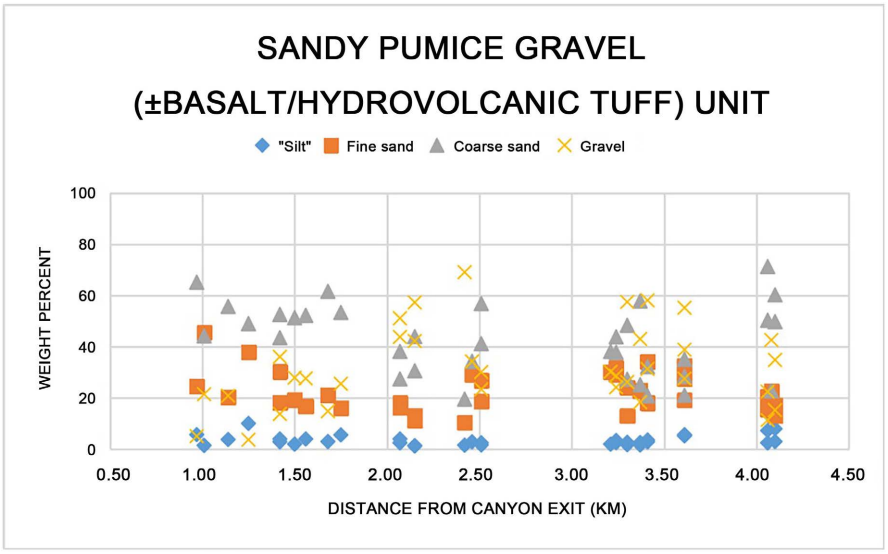

Figure 12. Weight percentages with respect to distance (km) from the canyon exit for the sandy pumice gravel (±basalt/hydrovolcanic tuff) unit. "Silt" = <0.07 mm; fine sand = ≥0.07 mm <0.42 mm; coarse sand = ≥0.42 mm <2.00 mm; gravel ≥2.00 mm. Average weight percent: "silt" = 3.6%, std. dev. = 2.5; fine sand = 22.4%, std. dev. = 8.0; coarse sand = 42.5%, std. dev. = 13.8; gravel = 31.7%, std. dev. 15.8.

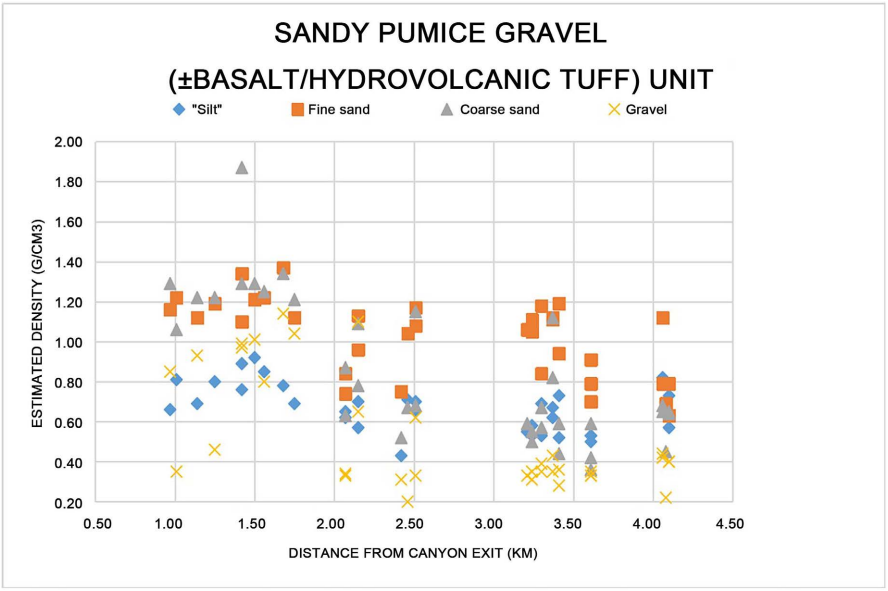

Figure 13. Estimated densities (g/cm^3) with respect to distance (km) from the canyon exit for samples of the sandy pumice gravel (±basalt/hydrovolcanic tuff) unit. "Silt" = <0.07 mm; fine sand = ≥0.07 mm <0.42 mm; coarse sand = ≥0.42 mm <2.00 mm; gravel ≥2.00 mm. Average estimated density: "silt" = 0.7 g/cm^3, std. dev. = 0.1; fine sand = 1.0 g/cm^3, std. dev. = 0.2; coarse sand = 0.8 g/cm^3, std. dev. = 0.4; gravel = 0.5 g/cm^3, std. dev. = 0.3.

and relative proportion of compositional components in the four size groupings. As an example, samples collected roughly 4 km from the canyon exit have high weight percentages of coarse-grained sand (Figure 12) but low estimated densities (Figure 13) consistent with the abundance of pumice in this size grouping.

Likewise, the relative paucity of fine-grained sand is reflected in lower weight percentages, but the higher estimated densities are consistent with crystals concentrated in this size grouping. With these examples in mind, changes are noted in the weight percentages and estimated densities in size groupings at about 2.0 km and about 3.6 km. The changes at 2.0 km occur where the abundance of basalt/hydrovolcanic tuff decreased and the abundance of pumice increased in gravel and coarse-grained sand. Beyond the pyroclastic flows exposed at 3.4 km and 3.7 km 1) fine-grain sizes (pan + 0.07 mm) were enriched, 2) coarse-grained mode in bimodal samples occurred in coarse sand (0.84 mm), and 3) pumice gravel decreased.

3) Pumice Pebble-bearing, Crystal-rich Sand The pumice pebble-bearing, crystal-rich sand unit (>70 wt. % ≥0.07 mm <2.00 mm) is present 1) along both flanks of the exposed boulder core between 0.9 and 1.2 km and 2) between about 1.5 km and 3.5 km. In the first case, the unit is the first encountered beneath a thin lag where the paleosurface had been eroded by migration of the Williamson River. In the second, the unit was exposed where the paleosurface of the debris fan is preserved. Characteristics of the pumice pebble-bearing, crystal-rich sand unit are summarized in Table 1.

Both flanks of the bedrock boulder core between 0.9 *and* 1.2 *km.* Distinctly better sorted (σ_1 = 0.68Φ to 1.02Φ), medium to coarse-grained sand (M_z = +0.90Φ to +1.21Φ) was present on both flanks of the boulder core near the canyon exit (0.9 to 1.2 km; moderately sorted sand in Figure 11). Four samples contained 95 to 100 weight percent sand (≥0.07 mm <2.00 mm) with 67.8 to 86.3 weight percent retained as medium-grained sand (0.25 mm + 0.42 mm). Estimated densities for all size fractions from 0.07 mm to 0.84 mm were between 1.2 and 1.4 g/cm^3, consistent with abundant crystals, compact glass, and micro vesiculated pumice. However, determining composition was difficult due to dark brown "silt" coatings on all grains. Similar coatings were described by [35] on re-sedimented pumice clasts from the Taupo ignimbrite eruption. There, coatings, "filter-cake", were interpreted to be "generated by infiltration of sediment-laden interstitial water into porous clasts".

The stratigraphic relations between the boulder core and these moderately well- to moderately sorted sands are suggested by three auger holes on the east flank of the core (Figure 11, 4724/4097, 4727/4097, 4758/4101). Over a distance of about 40 m and nearly constant surface elevation, the depth to the boulder core increased from 23 cm to greater than 125 cm. These stratigraphic relations were also present in auger hole 4407/4334 (Figure 11, refusal at 108 cm) located west of exposed boulders. These sites are approximately 400 m apart. Stratigraphic relations suggested that the sandy pumice gravel (±basalt/hydrovolcanic tuff) unit separates the moderately sorted, pumice pebble-bearing, crystal-rich sand unit from the boulder core. The contacts between sand units and boulder core appear to be relatively abrupt and steeply dipping.

Between about 1.5 *km and* 3.5 *km.* Figure 11 shows the distribution of auger holes between about 1.5 km and 3.5 km where the pumice pebble-bearing, crys-

tal-rich sand unit is present. Two subgroups are distinguished. The most common occurrence where remnants of the paleosurface are preserved is 1) upward grading of the sandy pumice gravel (±basalt/hydrovolcanic tuff) unit into the pumice pebble-bearing, crystal-rich sand unit. 2) Less common are auger holes where only the pumice pebble-bearing, crystal-rich sand is present. However, in some of these auger holes, depth of penetration may not have been great enough to enter the underlying sandy pumice gravel (±basalt/hydrovolcanic tuff) unit, if present.

The transition from the sandy pumice gravel (±basalt/hydrovolcanic tuff) to the pumice pebble-bearing, crystal-rich sand unit is characterized by 1) decreased mean grain size (M_z), 2) improved sorting (σ_I), 3) decreased weight percent gravel, 4) increased estimated density, and 5) retention of greatest mass to finer sieves. These changes are illustrated by two auger holes (3341/3898 (2.15 km) and 2525/2853 (3.41 km)) located approximately 1.3 km apart in an area where isolated pumice boulders rest upon the modern surface. The vertical and lateral trends in these auger holes are accounted for by the relative abundances of pumices and crystals. Rounded pumice cobbles were present in 2525/2853 where a rounded 5 cm diameter cobble was returned from about 100 cm depth. Pumice cobbles were rare in auger holes, but where present, they were recovered in only one auger run suggesting they may be present as discrete "lenses" within the pumice pebble-bearing, crystal-rich sand unit. Rounded pumice pebbles and cobbles in sand-sized matrix were noted by [30] in materials deposited by hyperconcentrated flows.

Pre-eruption topography of the Williamson River valley was suggested near the south edge of the debris fan. Observations at two groups of auger holes (Group 1 3348/2853, 3195/2957; Group 2 3561/3655, 3693/3582, and 3817/3420) suggested a pre-eruption side channel was present and the boulder core, sandy pumice gravel (±basalt/hydrovolcanic tuff), and pumice pebble-bearing, crystal-rich sand units were deposited in it.

The weight percentages and estimated densities relative to distance from the canyon exit for the pumice pebble-bearing, crystal-rich sand unit are presented in **Figure 14** and **Figure 15**, respectively. The four moderately to moderately well-sorted samples collected between 0.9 km and 1.2 km (**Figure 11**) had the lowest weight percentages of "silt" and gravel. These four samples had some of the highest estimated densities for the grain size groups. For all other samples, weight percentages by grain size groups are roughly similar across distance. Estimated densities by grain size groups were also similar with respect to distance. The exception was a single sample (2006/2459, 68-72 cm) located downstream from pyroclastic flows (>3.7 km).

5.4. Interpretive Cross Sections

Four cross sections constructed at 1.3 km (A-A'), 2.1 km (B-B') (**Figure 16**), 3.4 km (C-C') and 4.1 km (D-D') (**Figure 17**) summarize inferred stratigraphic relations.

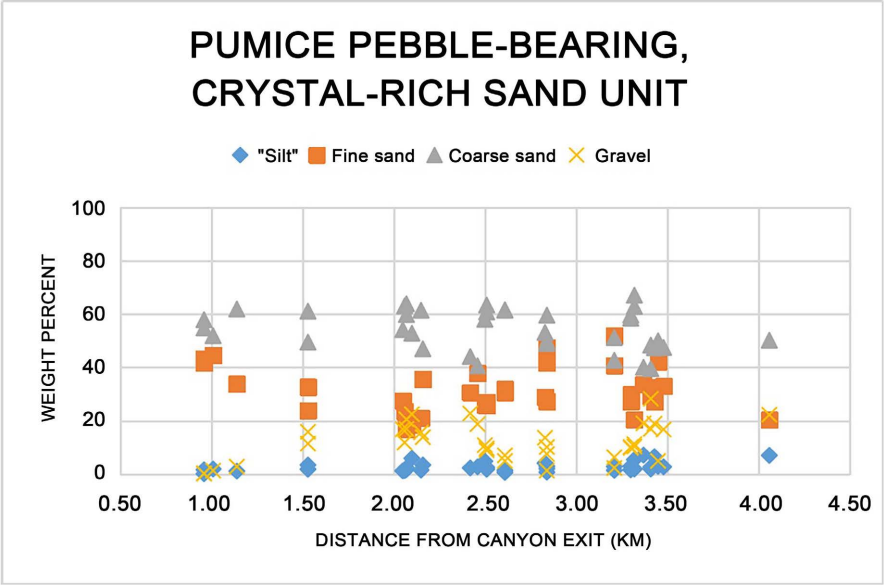

Figure 14. Weight percentages with respect to distance (km) from the canyon exit for the pumice pebble-bearing, crystal-rich sand unit. "Silt" = <0.07 mm; fine sand = ≥0.07 mm <0.42 mm; coarse sand = ≥0.42 mm <2.00 mm; gravel ≥2.00 mm. Average weight percent: "silt": 2.8 wt. %, std. dev. = 1.8; fine sand: 31.0 wt. %, std. dev. = 8.8; coarse sand: 59.2 wt. %, std. dev. = 7.6; gravel: 12.0 wt. %, std. dev. = 7.1.

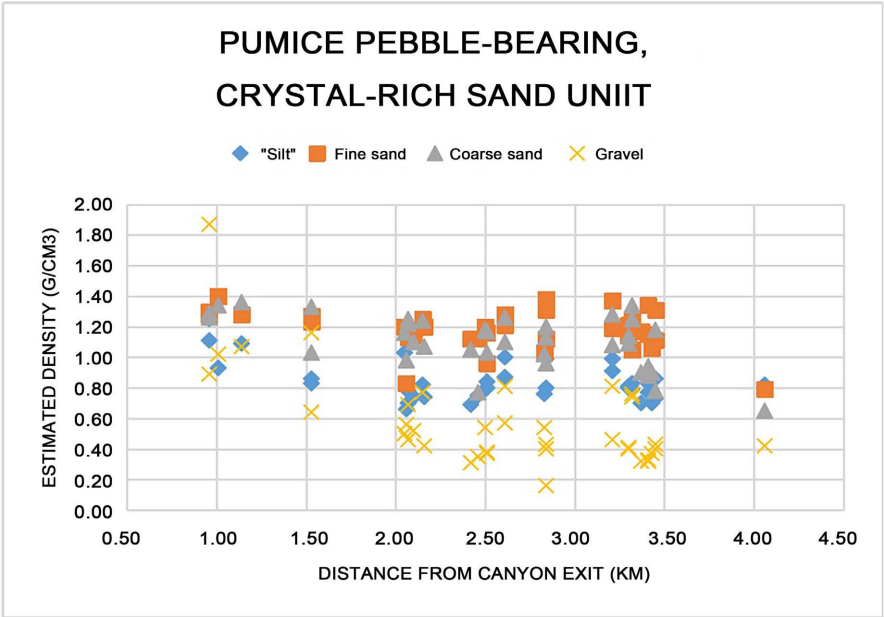

Figure 15. Estimated densities (g/cm^3) with respect to distance (km) from the canyon exit for samples of the pumice pebble-bearing, crystal-rich sand unit. "Silt" = <0.07 mm; fine sand = ≥0.07 mm <0.42 mm; coarse sand = ≥0.42 mm <2.00 mm; gravel ≥2.00 mm. Average estimated density: "silt" = 0.8 g/cm^3, std. dev. = 0.1; fine sand = 1.2 g/cm^3, std. dev. = 0.1; coarse sand = 1.1 g/cm^3, std. dev. = 0.2; gravel = 0.6 g/cm^3, std. dev. = 0.3.

5.4.1. Cross Section A-A'

Cross section A-A' (**Figure 16**) is located approximately 1.3 km into the boulder core. Here, boulders are exposed where the Williamson River channel crosses

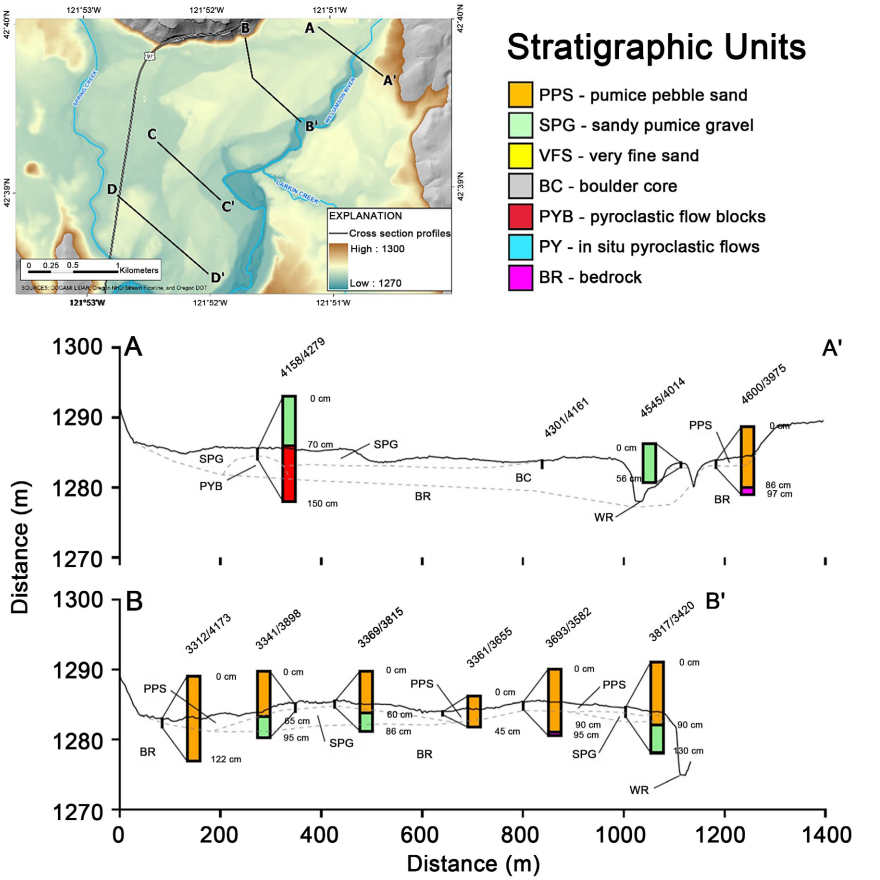

Figure 16. Location map and key for cross sections A-A' and B-B'. The location map and key also apply to cross sections shown in **Figure 17** (C-C' and D-D').

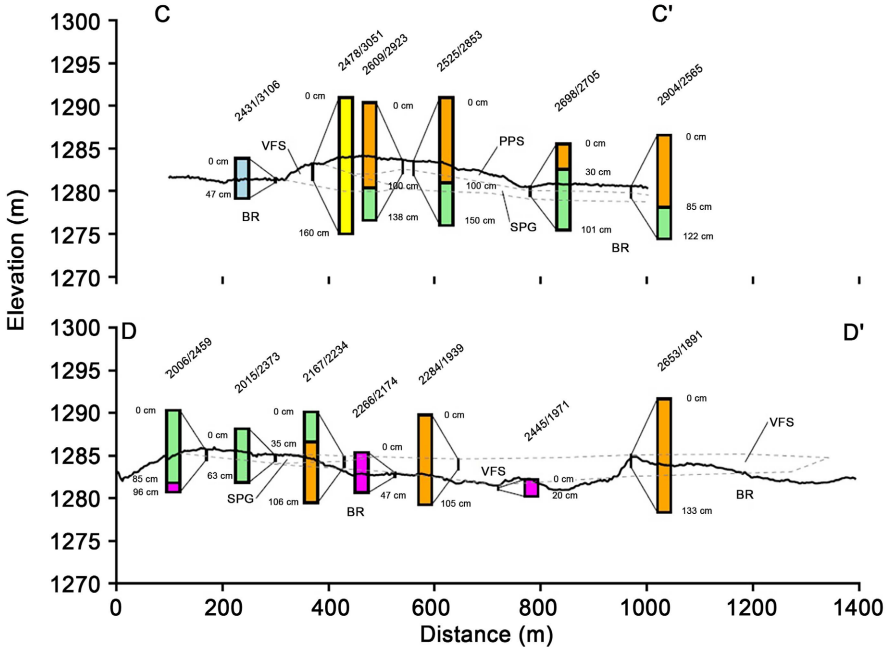

Figure 17. Cross sections C-C' and D-D'. Location of cross sections and key are provided in Figure 16.

the core (Figure 4). Two auger holes, 4600/3975 and 4158/4279, were 536 m apart on opposite sides of the boulder core. In auger hole 4600/3975, 85 cm of moderately (σ_1 = 0.68) to marginally poorly sorted (σ_1 = 1.02Φ), coarse-grained (M_z = +0.90Φ) sand overlies hydrovolcanic tuff bedrock. Here, deposition occurred in an overbank setting. The bank of the pre-eruption river is inferred to be 40 to 50 m away where a modern ravine bounds the east edge of the boulder core. In auger hole 4545/4014, 56 cm of poorly sorted (σ_1 = 1.65Φ), basalt pebble-bearing, coarse-grained sand (M_z = +0.21Φ) overlies the boulder core. Auger hole 4158/4279 located on the opposite side of the boulder core penetrated 70 cm of poorly sorted (σ_1 = 1.47Φ), strongly fine skewed (Sk_1 = 0.31), medium-grained (M_z = +1.55Φ) sand before it entered pyroclastic flows from 70 cm to 150 cm (E.O.H.) (samples 81 - 84 cm and 146 - 150 cm). Two explanations account for pyroclastic flows at the 4158/4279 site. 1) During the eruption, pyroclastic flows passed through the canyon and came to rest there, or 2) blocks of pyroclastic flows dislodged from within the canyon were transported to that location.

5.4.2. Cross Section B-B'

Cross section B-B' (Figure 16) was constructed 250 m down valley from the last boulder-bearing slash-burn pile and 2.1 km from the canyon exit. The cross section extends from near the base of slope that rises to US Highway 97 on the north end (B in Figure 16) to the modern incised channel of the Williamson River (B' in Figure 16) on the south, a distance of 1000+ m.

Tuffaceous sandy siltstone bedrock underlies the debris fan and forms a subsurface ridge at auger hole 3693/3582 separating what is interpreted as the main pre-eruption channel and floodplain of the Williamson River from a smaller side channel. The debris fan was characterized by sandy pumice gravel (±basalt/hydrovolcanic tuff) grading upward to pumice pebble-bearing, crystal-rich sand. Basalt and hydrovolcanic tuff are present as pebbles and coarse-grained sand in all but auger hole 3312/4173. Refusal at 95 cm in auger hole 3341/3898 (2.15 km) in the inferred main channel of the pre-eruption river is interpreted as an isolated boulder of bedrock embedded in sandy pumice gravel. Likewise, refusal at 111 cm in auger hole 3639/2994 (2.50 km, downstream from line of section) in the inferred side channel is interpreted as an isolated bedrock boulder embedded in sandy pumice gravel. An abandoned post-flood channel eroded the valley where auger hole 3561/3655 was located.

5.4.3. Cross Section C-C'

Cross section C-C' (Figure 17) was approximately 3.4 km from the canyon exit and crossed the ridge where local relief was nearly 3 m. Width of the deposit was less than 950 m constrained by auger hole 2431/3106 (Figure 7) in pyroclastic flows on the north side and auger hole 3348/2857 in tuffaceous siltstone bedrock on the south side (Figure 11).

Pyroclastic flows that overshot the basalt-rimmed plateau to the north during

the eruption of Mount Mazama were recovered from auger hole 2431/3106 and likely underlie the debris fan in part of this area. The *in situ* pyroclastic flows underlie the fine-grained sand unit (2478/3051) that forms a subtle bench located on the north flank of the ridge. These, in turn, are overlain by the sandy pumice gravel (±basalt/hydrovolcanic tuff) unit that grades upward to the pumice pebble-bearing, crystal-rich sand unit. Interstratified sandy pumice gravel and pumice pebble-bearing sand on the south flank of the ridge suggest interfingering of deposits emplaced in the main and side channels of the pre-eruption river valley.

5.4.4. Cross Section D-D'

Cross section D-D' (**Figure 17**) is located about 4.1 km from the canyon exit and downstream from pyroclastic flows at 3.5 km (**Figure 7**) and 3.7 km (2323/2583). The post-flood paleosurface is dissected by ephemeral stream valleys incised to weakly indurated tuffaceous sandy siltstone bedrock. The thickness of the deposit appears greater to the south (130 to 150 cm) and is interpreted to occupy the pre-eruption channel and floodplain of the Williamson River. To the north, the deposit appears thinner (85 cm in auger hole 2006/2373, **Figure 11**) and is interpreted to be overbank.

Auger hole 2167/2234 (4.08 km) (**Figure 7**) was important in defining stratigraphic relations in this cross section. The shallow sample from this hole (37 - 41 cm) was similar to samples recovered from auger holes to the north while the deeper samples (75 - 80 cm, 94 - 99 cm) were similar to those to the south. The sandy pumice gravel (±basalt/hydrovolcanic tuff) unit, but with elevated mass concentrations retained on the 0.07 mm sieve, was prominent to the north while the fine-grained sand unit was prominent to the south.

6. Discussion

Capra [36] summarized natural volcanic dams and discussed factors that contribute to stability and the deposits formed from their failure. O'Connor *et al.* [37] summarized dams and floods directly related to volcanism (e.g., [38]) and outburst floods due to drainage disruption from primary volcanic materials (e.g., [30]). Debris avalanches during eruptions are commonly associated with these floods [36]. Examples considered by [36] [37] and [39] emphasize disruption of drainage systems where relief is a significant characteristic of the volcanic landscape. In some cases, pyroclastic deposits near the volcanic source were breached to release large outburst floods [30] [34] [35] [39] [40] [41] [42]. Few examples of outburst floods from the breach of unwelded pyroclastic blockages distal from the volcanic source have been reported [10] [11] [12] [13].

Drainage disruptions produced by volcanic processes commonly occur at scales that leave distinct geologic records (e.g., [26] [29] [30] [31] [39] [41] [42] [43] [44]). However, drainage disruptions far from the volcanic source may leave only subtle topography and thin, low-volume deposits. Such is the case for two outburst floods associated with the middle Holocene eruption of Mount Maza-

ma. In these cases, narrow bedrock-lined canyons became blocked leading to the impoundment of lakes in low-relief landscapes [10] [11] [12] [13]. In this discussion the debris fan downstream from the Williamson River canyon is interpreted in relation to formation of the dam within the canyon, its removal, and the volume of material available for transport.

6.1. Dam Formation and Removal

The pyroclastic flows that blocked the canyon of the Williamson River entered the canyon after traveling approximately 35 km from the source volcano, Mount Mazama, across a relatively low relief landscape that had previously hosted a Pleistocene lake [12] [45]. Local topography (**Figure 2**) funneled pyroclastic flows into the canyon and across the neighboring lava flow-capped plateau. Shortly before the arrival of pyroclastic flows, Plinian pumice fall blanketed the area. The location of the canyon relative to the depositional axis of the eastern lobe of the Plinian pumice fall [1] [2] was characterized by thinning from north to south through the canyon. Thus, during the eruption the canyon came to be blanketed by a thin layer of Plinian pumice fall and filled (upper reaches) to partially filled (lower reaches) by ash-rich pyroclastic flows. The blockage in the canyon impounded a shallow lake with maximum surface area of 590 km^2. The maximum local depth was roughly estimated at 30 m and volume estimated at 5.7×10^9 m^3 [12] [13]. Overtopping followed by rapid breach growth is commonly inferred and documented as the processes leading to debris dam failures (e.g., [30] [41] [44]. Field observations of basalt bedrock exposed from approximately 1391 m to 1397 m on the west bank of the Williamson River canyon across from point RR in **Figure 2** suggest overtopping may have started in this area where Plinian pumice fall and pyroclastic flows have been stripped [13].

The narrow bedrock-lined canyon, non-welded pyroclastic flows, and the debris fan that formed downstream from the canyon exit when the blockage failed have similarities to the much larger system formed along the Waikato River after the 1.8 ka eruption of the Taupo caldera, North Island, New Zealand [29] [41]. There, non-welded ignimbrite blocked the narrow outlet gorge of the pre-eruption lake that occupied the caldera. A post-eruption lake filled the caldera, overtopped the debris dam, and cut a 12 km-long narrow canyon. Downstream from the canyon, a bouldery debris fan formed where the flood emerged from the canyon into the low-gradient Reporoa basin [41].

6.2. Units of the Debris Fan

Five units provide insight into processes that occurred during clearing of debris from the Williamson River canyon. These are: 1) bedrock boulders at distances up to 2.50 km, 2) fine-grained sand unit, 3) pyroclastic flows at 3.34 km, 3.5 km, and 3.7 km, 4) sandy pumice gravel (±basalt/hydrovolcanic tuff) and pumice-bearing crystal-rich sand units, and 5) moderately well- to moderately sorted sand near the canyon exit.

6.2.1. Bedrock Boulders at Distances up to 2.50 km

Bedrock boulders were sourced at least as far up canyon as outcrops of the texturally distinct olivine basalt (near RR in **Figure 2**), approximately 4 km. These texturally distinct boulders (**Figure 5(a)**, **Figure 5(b)**) are present on slash-burn piles at least 1.9 km from the canyon exit. Outcrops of hydrovolcanic tuff in the lower 2.6 km of the canyon (starting near the distinct bend in the middle canyon, **Figure 2**) were the sources of hydrovolcanic tuff boulders (**Figure 6**) that were also deposited at least 1.9 km (slash-burn piles) from the canyon exit. Basalt flows were too widely distributed to yield information on source or distance of transport. Near 1.1 km the eastern edge of the deposit was controlled by pre-eruption topography (**Figure 16**). At 1.3 km the boulder core is 420 m wide, 4 to 6 m thick, and its edges are relatively abrupt. The boulders are inferred to be embedded in lithic-rich sand and gravel similar to the sandy pumice gravel (±basalt/hydrovolcanic tuff) unit. The size and abundance of bedrock boulders decrease with distance from the canyon exit. Refusal against isolated boulders embedded within the sandy pumice gravel (±basalt/hydrovolcanic tuff) unit extends at least 2.50 km.

Co-deposition of boulders and pumice sand was hypothesized by [41] where the outburst flood on the Waikato River spread out in the Reporoa basin. In this setting deceleration and shallowing lead to boulder deposition as flow competence decreased and matrix deposition as flow capacity decreased. Likewise, the bedrock lined Williamson River canyon opens into a low relief broad valley (**Figure 2**) where bedrock boulders and matrix came to rest in the pre-eruption channels and flood plain.

6.2.2. Fine-Grained Sand Unit

In addition to similarities to samples from pyroclastic flows, the fine-grained sand unit was recovered from three settings: 1) deepest samples from three auger holes upstream from pyroclastic flows (<3.5 km) where it was overlain by sandy pumice gravel (±basalt/hydrovolcanic tuff), 2) exposed at the surface on a subtle bench upstream from pyroclastic flows (<3.5 km) where it was at least 160 cm thick and inferred to overlie *in situ* pyroclastic flows, and 3) exposed at the surface downstream from pyroclastic flows (>3.7 km) where it was greater than 130 cm thick and inferred to overlie tuffaceous silty sandstone. Stratigraphy, topography, and statistical parameters of grain size suggest the fine-grained sand unit was rapidly deposited with minimal reworking of remobilized pyroclastics sourced from 1) *in situ* pyroclastic flows, or 2) from within the canyon. Manville [29] describes similarities between primary and secondary ignimbrites from the AD 181 Taupo eruption and facies B, pumiceous diamict, as due to mass-flow remobilization of the ignimbrites. In the case of the Williamson River debris fan, the fine-grained sand unit is interpreted to be pyroclastic-flow materials remobilized during the outburst flood. Deposition may have been contemporaneous with emplacement of the boulder core, but prior to the onset of hyperconcentrated flows that deposited the sandy pumice gravel (±basalt/hydrovolcanic tuff)

and pumice pebble-bearing, crystal-rich sand unit.

6.2.3. Pyroclastic Flows at 3.34 km, 3.5 km, and 3.7 km

Three sites along the north flank of the debris fan illustrate relations between the debris fan and *in situ* pyroclastic flow deposits. At 3.34 km, the width of the debris fan is less than 950 m, the distance from auger hole 2431/3106 in pyroclastic flows on the north side and 3348/2857 in tuffaceous siltstone on the south side. At 3.5 km the contact between *in situ* pyroclastic flows and sandy pumice gravel (±basalt/hydrovolcanic tuff) unit is sharp (**Figure 8**). The characteristics of the contact suggest erosion at the base of the debris fan. At 3.7 km, *in situ* pyroclastic flows exposed in an ephemeral stream valley are overlain by pumice gravel of the sandy pumice gravel (±basalt/hydrovolcanic tuff) unit, but the contact is not exposed. The pyroclastic flow deposits crossed the plateau west of the Williamson River canyon, overshot the south rim of the plateau, and came to rest at these three sites. Likewise, an increase in "silt" and fine-grained sand in the pumice pebble-bearing, crystal-rich sand unit downstream from the 3.5 km and 3.7 km sites (**Figure 14** and **Figure 15**) suggests upstream entrainment of ash from these pyroclastic flow deposits.

6.2.4. Sandy Pumice Gravel (±Basalt/Hydrovolcanic Tuff) and Pumice Pebble-Bearing, Crystal-Rich Sand

The sandy pumice gravel (±basalt/hydrovolcanic tuff) and pumice pebble-bearing, crystal-rich sand units are interpreted as hyperconcentrated flow deposits based on mean grain size (M_z), sorting, mass distribution with respect to grain size, composition, and estimated densities. These deposits were not associated with debris-flow deposits but locally may have transitioned to normal stream-flow deposits. Characteristics commonly relied upon to infer transport and depositional processes such as bedding, pebble/cobble orientations and imbrication, and grain size distribution determined from outcrops (e.g. [46]) could not be documented. Straight-grained, rounded wood fragments were present in the sandy pumice gravel. Scott [47] interpreted the concentration of low-density wood fragments and pumice near the base of some 1982 and pre-1980 hyperconcentrated flow deposits from Mount St. Helens as indicating "extremely rapid deposition from a hyperconcentrated flood surge". Hyperconcentrated flows that discharged from the canyon followed the main and side channels of the pre-eruption Williamson River. Deposits within the main and side channels may interfinger across the bedrock high (**Figure 16**) that separates these two flow paths and suggests progressive collapse of the blockage within the canyon may have sent pulses of hyperconcentrated flows onto the debris fan.

Benvenuti and Matini [46] reviewed terms used to describe hyperconcentrated flows and their deposits in terrestrial settings. The terms are applied to flow dynamics and deposits formed in the transition from debris flows to normal stream flow with usage drawing attention to the flow dynamics and deposit characteristics emphasized by researchers (e.g., [25] [26] [27] [30] [47]).

The statistical parameters of grain size [32] reported in this study are similar to those determined for hyperconcentrated flows at Mount St. Helens [26] [47] and El Chichón [30]. Analysis of the lahar-runout deposits from May 18-19, 1980 and direct measurement of sediment concentrations from hyperconcentrated flows during the March 19, 1982 explosive eruption of Mount St. Helens constrained the flow regime needed for hyperconcentrated flow [26] [47]. These deposits had coarse sandy texture, mean grain size (M_z) from +0.9Φ to +1.6Φ and were poorly sorted ((σ_1) 1.1Φ to 1.6Φ). Macías *et al.* [30] analyzed hyperconcentrated flow-deposits along the Magdalena River that formed during the breakout flood of May 26, 1982. This flood originated from a lake impounded behind a dam of pyroclastic debris formed during the eruption of El Chichón [40]. Macías *et al.* [30] indicated that the hyperconcentrated-flow deposit "consists mainly of centimeter-sized rounded pumices and crystals". Downstream, mean grain size (M_z) decreased from +1.3Φ to +2.7Φ as sorting (σ_1) improved from 1.1Φ to 0.7Φ. Characteristics of the hyperconcentrated flow deposits from the debris fan in this study are similar to those described by [6] [25] [30] and [47] in that they were clast supported, had medium to coarse sandy texture, M_z ranged from −1.48Φ to +2.10Φ, sorting (σ_1) from 0.68Φ to 2.54Φ and relatively low weight percentages of very fine-grained sand and silt (<0.07 mm) (**Table 1**).

6.2.5. Moderately Well- to Moderately Sorted Sand near Canyon Exit

Localized moderately well-sorted sand (0.9 - 1.2 km) on both sides of the bedrock boulder core near the canyon exit are distinctly different from other sandy units of the debris fan. These moderately well- to moderately sorted, higher estimated density, medium- to coarse-grained lithic and crystal-rich sands appear to be the last debris moving onto the debris fan from the canyon and may reflect better sorting as transport distance increased and the supply of pyroclastic debris neared exhaustion. The ash-rich pyroclastics in the canyon were rapidly eroded as the impounded lake drained. Each turbulent pulse of hyperconcentrated flows presumably was generated by partial collapses of the blockage in the canyon. Each collapse added to the distance of transport within the narrow canyon allowing better sorting on the debris fan. Once the blockage was removed from within the canyon less material became available for transport (discussed below).

A second area where the better sorted (1.01Φ to 1.22Φ) pumice pebble-bearing, crystal-rich sand unit is present is upstream of pyroclastic flows at 3.5 km (roughly 2.6 to 3.2 km). Better sorting and increased estimated density suggest conditions may have approached transition to normal stream flow where these sands were deposited.

6.3. Volume Available for Transport

The volume of pyroclastics available for transport during removal of the blockage in the Williamson River canyon was originally stored in three settings. 1) Upstream from the knickpoint was the broad, low relief landscape now hosting Klamath Marsh (**Figure 1**). This area, directly east of Mount Mazama, was

where a significant volume of pyroclastic flows was deposited during the eruption (9 to 18+ m thick). However, the bedrock knickpoint (elevation ~1368 m) at the head of the canyon restricted the volume released from this area. 2) Between the knickpoint and about 2 km where the narrow bedrock-lined portion of the canyon begins (**Figure 2**) was a topographic depression bounded on the north by the lava flow that formed the knickpoint, on the east by Soloman Butte, and on the west by low volume lava flows and vent deposits [14] [48]. In this topographic depression, pyroclastic flows may have been between 15 and 24 m thick. However, only a portion of this volume was removed during draining of the lake as suggested by: a) remnants of the lake bed where settled pumice pebbles overlie pyroclastic flows (elevation 1378 m; [13]; similar to facies F of [29], b) 1 km^2 raft of stranded pumice boulders (up to 25 cm diameter) between 1378 and 1384 m [14], c) radially oriented, narrow, stream-less valleys cut 5 to 10 m into settled pumice and underlying pyroclastic flows that formed during draining of the lake (**Figure 2**). 3) The 5 km long, narrow, bedrock-lined canyon downstream was filled (~60 to 70 m thick) to partially filled (lower reach of the canyon) by pyroclastic flows. The estimated volume of the pyroclastic dam, 0.04 km^3 to 0.08 km^3, was primarily resident in the latter two settings. This relatively small volume of ash-rich pyroclastics was removed as the impounded lake drained through the canyon.

7. Conclusions

Narrow, bedrock-lined canyons distal from a source volcano can be blocked by ash-rich pyroclastic flows [12] [13] or wind re-worked Plinian pumice fall [10] [11]. Outburst floods from shallow lakes impounded by these blockages likely occur by overtopping and rapid erosion of the ash-rich pyroclastic deposits that filled the canyons.

Pyroclastic flows from the eruption of Mount Mazama traveled at least 35 km before entering the bedrock-lined canyon of the Williamson River. Ash-rich pyroclastic flows filled the upper canyon and partially filled the lower canyon.

The volume available for transport in an outburst flood was relatively small (0.04 km^3 to 0.08 km^3) and controlled by the width, depth, length, and location of the knickpoint at the head of the canyon. Outburst floods far from the volcanic source may leave debris fans with subtle topography and thin, low-volume deposits.

Co-deposition of bedrock boulders and pumice-bearing, lithic-rich pebbles and coarse-grained sand occurred where the canyon opened into a broad, low-relief valley. The thickness of this unit decreased, and the intermediate diameter of individual boulders decreased away from the canyon exit. The farthest transport distance of bedrock boulders is estimated at 2.5 km where isolated boulders are inferred to be hosted within the sandy pumice gravel (±basalt/hydrovolcanic tuff) unit.

Deposition of fine-grained sand coincided with emplacement of the boulder

core. Statistical parameters of grain size, crystal and pumice pebble abundance, and estimated density by grain sizes were similar to pyroclastic flows and suggest limited working and rapid deposition contemporaneously with emplacement of the boulder core.

Where the post outburst flood surface is preserved, the poorly sorted sandy pumice gravel (±basalt/ hydrovolcanic tuff) unit grades upward into the pumice pebble-bearing crystal-rich sand unit. Total thickness is estimated between 1.5 and 3 m. Coarse-grained sand and pebbles of basalt and hydrovolcanic tuff decrease in abundance with increased distance from the canyon exit and are absent beyond about 2.3 km. Pumice pebbles increase in abundance and locally comprise more than 20 weight % of the sandy pumice gravel (±basalt/hydrovolcanic tuff) unit. These sand-rich units were deposited by hyperconcentrated flows generated during collapses of the debris dam within the canyon. Locally, hyperconcentrated flows approached normal stream flow conditions when the pumice pebble-bearing, crystal-rich sand unit was deposited. Upward fining from poorly sorted pumice-rich gravel to poorly sorted crystal-rich sand was accompanied by increased estimated density of sand.

Progressive upstream failure of the dam increased the distance of transport until the supply of pyroclastics was exhausted. Increased transport distance improved sorting and resulted in deposition of moderately sorted, lithic- and crystal-rich sand near the canyon exit.

Acknowledgements

David Eibert prepared the figures used in this paper. James O'Connor provided a helpful review that improved the length and focus of the paper.

Conflicts of Interest

The author declares no conflicts of interest regarding the publication of this paper.

References

[1] Williams, H. (1942) The Geology of Crater Lake National Park, Oregon. Carnegie Institute of Washington, Washington.

[2] Young, S.R. (1990) Physical Volcanology of Holocene Airfall Deposits from Mt. Mazama, Crater Lake, Oregon. Ph.D. Thesis, University of Lancaster, Lancaster.

[3] Zdanowicz, C.M., Zielinski, G.A. and Germani, M.S. (1999) Mount Mazama Eruption: Calendrical Age Verified and Atmospheric Impact Assessed. *Geology*, **27**, 621-624. https://doi.org/10.1130/0091-7613(1999)027<0621:MMECAV>2.3.CO;2

[4] Bacon, C.R. and Lanphere, M.A. (2006) Eruptive History and Geochronology of Mount Mazama and the Crater Lake Region, Oregon. *Geological Society of America Bulletin*, **118**, 1331-1359. https://doi.org/10.1130/B25906.1

[5] Bacon, C.R. (2008) Geologic Map of Mount Mazama and Crater Lake Caldera, Oregon. U.S. Geological Survey Scientific Investigations Map 2832, scale 1:24,000.

[6] Jenks, M.D. (2007) Geologic Compilation Map of Part of the Upper Klamath Basin,

Klamath County, Oregon. Open-File Report O-07-05, Oregon Department of Geology and Mineral Industries.

[7] Cummings, M.L. and Melady, J.S. (2002) Hydrogeology of the Klamath Marsh, Klamath County, Oregon. *Proceedings, Klamath Basin Fish & Water Management Symposium*, 2001.

[8] Alexander, K.A., Amos, C.B., Balco, G., Amidon, W.H., Lesnau, R.K., Clark, D. and Meigs, A. (2019) Rates and Kinematics of Active Crustal Faults in the Central Oregon Cascades. *Geological Society of America Abstracts with Programs*, **51**. https://doi.org/10.1130/abs/2019CD-329211

[9] Alexander, K. (2020) Slip Rates and Kinematics of Active Crustal Faults in the Central Oregon Cascades. M.S. Thesis, Western Washington University, Bellingham. https://cedar.wwu.edu/wwuet/947 https://doi.org/10.1130/abs/2019CD-329211

[10] Lind, P. (2009) Holocene Floodplain Development of the Lower Sycan River, Oregon. M.S. Thesis, University of Oregon, Eugene.

[11] O'Connor, J.E., McDowell, P.F., Lind, P., Rasmussen, C.G. and Keith, M.K. (2015) Geomorphology and Flood-Plain Vegetation of the Sprague and Lower Sycan Rivers, Klamath Basin, Oregon. U.S. Geological Survey Scientific Investigations Report 2014-5223. https://doi.org/10.3133/sir20145223

[12] Conaway, J.S. (1999) Hydrogeology and Paleohydrology in the Williamson River Basin, Klamath County, Oregon. M.S, Thesis, Portland State University, Portland. https://doi.org/10.15760/etd.3524

[13] Cummings, M.L. and Conaway, J.S. (2009) Landscape and Hydrologic Response in the Williamson River Basin Following the Holocene Eruption of Mount Mazama, Cascade Volcanic Arc. In: O'Connor, J.E., Dorsey, R.J., and Madin, I.P., Eds., *Volcanoes to Vineyards*: *Geologic Field Trips through the Dynamic Landscape of the Pacific Northwest*, Geological Society of America, Boulder, 271-294. https://doi.org/10.1130/2009.fld015(14)

[14] Lee, C.L. (2000) Magmatic Processes Operating during the Middle to Late Pliocene and Pleistocene Along the Cascades-Basin and Range Transition Zone Near 43˚ North. M.S. Thesis, Portland State University, Portland.

[15] Conaway, J.S. and Cummings, M.L. (1999) Mid-Holocene Flooding on the Williamson River, Klamath County, Oregon. *Geological Society of America Abstracts with Programs*, **31**, A46.

[16] Baker, V.R. and Ritter, D.F. (1975) Competence of Rivers to Transport Coarse Bed-load Material, *Geological Society of America Bulletin*, **86**, 975-978. https://doi.org/10.1130/0016-7606(1975)86<975:CORTTC>2.0.CO;2

[17] Costa, J.E. (1983) Paleohydraulic Reconstruction of Flash-Flood Peaks from Boulder Deposits in the Colorado Front Range. *Geological Society of America Bulletin*, **94**, 986-1004. https://doi.org/10.1130/0016-7606(1983)94<986:PROFPF>2.0.CO;2

[18] Komar, P.D. (1989) Flow-Competence Evaluations of the Hydraulic Parameters of Floods: An Assessment of the Technique. In: Beven, K. and Carling, P., Eds., *Floods-Hydrological*, *Sedimentological*, *and Geomorphological Implications*, John Wiley and Sons, Chichester, 107-134.

[19] O'Connor, J.E. (1993) Geological Society of America Special Paper 274. Geological Society of America, Boulder. https://doi.org/10.1130/SPE274-p1

[20] Costa, J.E. and Schuster, R.L. (1988) The Formation and Failure of Natural Dams. *Geological Society of America Bulletin*, **100**, 1054-1068. https://doi.org/10.1130/0016-7606(1988)100<1054:TFAFON>2.3.CO;2

[21] Walder, J.S. and O'Connor, J.E. (1997) Methods of Predicting Peak Discharge of Floods Caused by Failure of Natural and Constructed Earthen Dams. *Water Resources Research*, **33**, 2337-2348. https://doi.org/10.1029/97WR01616

[22] O'Connor, J.E. and Beebee, R.A. (2009) Floods from Natural Rock-Material Dams. In: Burr, D.M., Carling, P.A. and Baker, V.R., Eds., *Megaflooding on Earth and Mars*, Cambridge University Press, Cambridge, 128-171. https://doi.org/10.1017/CBO9780511635632.008

[23] Froehlich, D.C. (1987) Embankment-Dam Breach Parameters. In: Ragan, R.M., Ed., *Proceedings of* 1987 *National Conference on Hydraulic Engineering*, *American Society of Civil Engineers*, New York, 570-575.

[24] Wahl, T.L. (2004) Uncertainty of Predictions of Embankment Dam Breach Parameters. *Journal of Hydraulic Engineering*, **130**, 389-397. https://doi.org/10.1061/(ASCE)0733-9429(2004)130:5(389)

[25] Nemec, W. and Muszynski, A. (1982) Volcaniclastic Alluvial Aprons in the Tertiary of Sofia District (Bulgaria). *Annales Societatis Geologorum Poloniae*, **52**, 239-303.

[26] Pierson, T.C. and Scott, K.M. (1985) Downstream Dilution of a Lahar: Transition from Debris Flow to Hyperconcentrated Streamflow. *Water Resources Research*, **21**, 1511-1524. https://doi.org/10.1029/WR021i010p01511

[27] Smith, G.A. (1986) Coarse-Grained Nonmarine Volcaniclastic Sediment: Terminology and Depositional Process. *Geological Society of America Bulletin*, **97**, 1-10. https://doi.org/10.1130/0016-7606(1986)97<1:CNVSTA>2.0.CO;2

[28] Park, C. and Schmincke, H.-U. (1997) Lake Formation and Catastrophic Dam Burst during the Late Pleistocene Laacher See Eruption (Germany). *Naturwissenschaften*, **84**, 521-525. https://doi.org/10.1007/s001140050438

[29] Manville, V. (2002) Sedimentary and Geomorphic Response to Ignimbrite Emplacement: Readjustment of the Waikato River after the AD 181 Taupo Eruption, New Zealand. *The Journal of Geology*, **110**, 519-542. https://doi.org/10.1086/341596

[30] Macías, J.L., Capra, L., Scott, K.M., Espadola, J.M., Garca-Palomo, A. and Costa, J.E. (2004) The 26 May 1982 Breakout Flows Derived from Failure of a Volcanic Dam at El Chichón, Chiapas, Mexico. *Geological Society of America Bulletin*, **116**, 233-246. https://doi.org/10.1130/B25318.1

[31] Hodgson, K.A. and Nairn. I.A. (2005) The c. AD 1315 Syn-Eruption and AD 1904 Post-Eruption Breakout Floods from Lake Tarawera, Haroharo Caldera, North Island, New Zealand. *New Zealand Journal of Geology & Geophysics*, **48**, 491-506. https://doi.org/10.1080/00288306.2005.9515128

[32] Folk, R.L. (1980) Petrology of Sedimentary Rocks. Hemphill Publishing Company, Austin.

[33] Smith, G.A. and Smith, R.D. (1985) Specific Gravity Characteristics of Recent Volcaniclastic Sediment: Implications for Sorting and Grain Size Analysis. *Journal of Geology*, **93**, 619-622. https://doi.org/10.1086/628986

[34] Manville, V., Segschneider, B. and White, J.D.L. (2002) Hydrodynamic Behavior of Taupo 1800a Pumice: Implications for the Sedimentology of Remobilized Pyroclasts. *Sedimentology*, **49**, 955-976. https://doi.org/10.1046/j.1365-3091.2002.00485.x

[35] Manville, V., Newton, E.H. and White, J.D.L. (2005) Fluvial Responses to Volcanism: Resedimentation of the 1800a Taupo Ignimbrite Eruption in the Rangitaiki River Catchment, North Island, New Zealand. *Geomorphology*, **65**, 49-70. https://doi.org/10.1016/j.geomorph.2004.07.007

[36] Capra, L. (2007) Volcanic Natural Dams: Identification, Stability, and Secondary

Effects. *Natural Hazards*, **43**, 45-61. https://doi.org/10.1007/s11069-006-9101-2

[37] O'Connor, J.E., Clague, J.J., Walder, J.S., Manville V. and Beebee, R.A. (2013) 9.25 Outburst Floods. In: Shroder, J. and Wohl, E.E., Eds., *Treatise on Geomorphology*, Academic Press, San Diego, 475-510. https://doi.org/10.1016/B978-0-12-374739-6.00251-7

[38] Pierson, T.C., Janda, R.J., Thouret, J-C. and Berrero, C.A. (1990) Perturbation and Melting of Snow and Ice by the 13 November 1985 Eruption of Nevada del Ruiz, Colombia, and Consequent Mobilization, Flow and Deposition of Lahars. *Journal of Volcanology and Geothermal Research*, **41**, 17-66. https://doi.org/10.1016/0377-0273(90)90082-Q

[39] Manville, V., Hodgson, K.A. and Nairn, I.A. (2007) A Review of Break-Out Floods from Volcanogenic Lakes in New Zealand. *New Zealand Journal of Geology and Geophysics*, **50**, 131-150. https://doi.org/10.1080/00288300709509826

[40] Macías, J.L., Sheridan, M.F. and Espadola, J.M. (1997) Reappraisal of the 1982 Eruptions of El Chichón Volcano, Chiapas, Mexico: New Data from Proximal Deposits. *Bulletin of Volcanology*, **58**, 459-471. https://doi.org/10.1007/s004450050155

[41] Manville, V., White, J.D.L., Houghton, B.F. and Wilson, C.J.N. (1999) Paleohydrology and Sedimentology of a Post-1.8 ka Breakout Flood from Intracaldera Lake Taupo, North Island, New Zealand. *Geological Society of America Bulletin*, **111**, 1435-1447. https://doi.org/10.1130/0016-7606(1999)111<1435:PASOAP>2.3.CO;2

[42] Kataoka, K.S., Urabe, A., Manville, V. and Kajiyama, A. (2008) Breakout Flood from an Ignimbrite-Dammed Valley after the 5 ka Numazawako Eruption, Northeast Japan. *Geological Society of America Bulletin*, **120**, 1233-1247. https://doi.org/10.1130/B26159.1

[43] Waythomas, C.F., Walder, J.S., McGimsey, R.G. and Neal, C.A. (1996) A Catastrophic Flood Caused by Drainage of a Caldera Lake at Aniakchak Volcano, Alaska, and Implications for Volcanic Hazards Assessment. *Geological Society of America Bulletin*, **108**, 861-871. https://doi.org/10.1130/0016-7606(1996)108<0861:ACFCBD>2.3.CO;2

[44] Waythomas, C.F. (2001) Formation and Failure of Volcanic Debris Dams in the Chakachatna River Valley Associated with Eruptions of the Spurr Volcanic Complex, Alaska. *Geomorphology*, **39**, 111-129. https://doi.org/10.1016/S0169-555X(00)00097-0

[45] Snyder, C.T., Hardman, G., and Zdeneck, F.F. (1964) Pleistocene Lakes in the Great Basin. U.S. Geological Survey Miscellaneous Geologic Investigations Map I-416, scale 1:1,000,000.

[46] Benvenuti, M. and Martini, I.P. (2002) Analysis of Terrestrial Hyperconcentrated Floods and Their Deposits. In: Martini, I.P., Baker, V.R. and Garzón, G., Eds., *Flood and Megaflood Processes and Deposits*: *Recent and Ancient Special Publication* 32, International Association of Sedimentologists, Bern, 167-193. https://doi.org/10.1002/9781444304299.ch10

[47] Scott, K.M. (1988) Origins, Behavior, and Sedimentology of Lahars and Lahar-Runout Flows in the Toutle-Cowlitz River System. U.S. Geological Survey Professional Paper 1447-A. https://doi.org/10.3133/pp1447A

[48] Wiley, T.J. (2004) Geologic Map of the Fort Klamath Quadrangle, Klamath County, Oregon. Oregon Department of Geology and Mineral Industries, GMS 96, Scale 1:24,000.